CHARACTERIZATION OF BAND 3 VARIANT G130R USING SITE-DIRECTED SPIN LABELING AND ELECTRON PARAMAGNETIC RESONANCE

by

Elizabeth Anne Nalani Nathaniel

Thesis

Submitted to the Faculty of the

Graduate School of Vanderbilt University

in partial fulfillment of requirements

for the degree of

MASTER OF SCIENCE

in

Chemical and Physical Biology

May, 2010

Nashville, Tennessee

To my parents for their continued support and understanding

ACKNOWLEDGMENTS

I would like to express my gratitude to all those who have given me help in recent years. I thank the Vanderbilt Medical Scientist Training Program for allowing me the opportunity to study at Vanderbilt. I am especially grateful to the Vanderbilt MSTP director, Dr. Terry Dermody, who was always willing to offer advice and support. I would also like to thank the National Institutes of Health for helping to fund this project.

I am indebted to my mentor and advisor, Dr. Al Beth. Without his continued support, both morally and financially, I would not have been able to complete this study. He has been patient and understanding, even when I was facing difficult times. I am also thankful to Suzanne Brandon for her assistance in protein preparation and purification. The DEER experiments were performed and analyzed by Dr. Eric Hustedt, contributing additional data regarding my project.

I would also like to thank those close to me who supported me during my time at Vanderbilt, especially my family. I appreciate the words of encouragement and occasional pushes offered by my mother. My father has always been supportive of my decisions and constantly patient with me. I would like to thank my older brother, Bobby, and older sister, Alexis, who have both been great friends to me. I also thank my little sisters, Kaila and Kalea, for brightening my life. Without the support of my family, I would have been lost.

TABLE OF CONTENTS

Page

List of Figures

CHAPTER I

INTRODUCTION

Rationale for Dissertation

Anion exchanger 1 (AEI), also known as band 3, is the most abundant integral membrane protein in the human erythrocyte (Fairbanks et al. 1971). Band 3 is composed of two structurally and functionally distinct domains (Steck et al. 1976). The transmembrane domain of band 3 (tdb3) is responsible for the exchange of chlorine and bicarbonate ions across the erythrocyte membrane (Cabantchik and Rothstein 1974), a process essential to CO_2 excretion and acid-base balance regulation in the blood (Crandall et al. 1981). The cytoplasmic domain of band 3 acts as an organizing center for numerous protein-protein interactions at the red blood cell membrane. Proteins that interact with cdb3 include membrane cytoskeleton components, glycolytic enzymes, hemoglobin, and hemichromes (Low 1986). Mutations in AE1 are associated with hereditary spherocytosis (HS) (Delaunay 2002) and Southeast Asian ovalocytosis (SAO) (Jarolim et al. 1991). The crystal structure of cdb3 (55-356) has been determined at the nonphysiological pH 4.8 (Zhang et al. 2000) and its solution structure at pH 6.8 confirmed the packed dimer structure observed in the crystal structure (Zhou et al. 2005).

Of the three mutations in the cytoplasmic domain that are associated with HS, only the Tuscaloosa variant (P327R) has been studied from the angle of structural biology (Zhou et al. 2007). The band 3 Fukuoka variant (G130R), like the P327R mutation, results in decreased protein 4.2 while having little effect on the

total band 3 content of the red blood cell. The G130R mutation is located on the surface of helix 2, a region thought to be part of the ankyrin-binding interface. This dissertation study utilizes site-directed spin labeling (SDSL) paired with electron paramagnetic resonance (EPR) techniques in order to study the structural changes caused by the G130R mutation. This work has shown that EPR methods can be advantageous when studying small structural changes by providing information on secondary structure and residue environment.

Erythrocyte Membrane Skeleton

Organization of the Erythrocyte Cytoskeleton

The erythrocyte membrane skeleton is well-studied and provides a model system for the study of protein-membrane interaction. The membrane skeleton is typically organized as a hexagonal lattice (Figure 1A) composed primarily of spectrin tetramers, formed by head-to-tail association of spectrin αβ heterodimers (Morrow and Marchesi 1981). The ends of the spectrin tetramers form junctional complexes with a number of proteins such as actin, protein 4.1, protein 4.9, tropomyosin, and adducin (Figure 1B) (Bennett 1989).

In addition to these associations, the erythrocyte cytoskeleton interacts with the red blood cell membrane through two multiprotein complexes. One of the complexes occurs at the aforementioned junctional complex involving spectrin, actin, and protein 4.1. At this site, protein 4.1 creates another ternary complex with protein p55 and the transmembrane protein glycophorin C, binding the spectrin network to the erythrocyte membrane (Figure 1B). Protein 4.1 can also interact

with the dimeric form of the integral membrane protein band 3 and has binding sites for the transmembrane proteins Rh, Kell, and XK (Salomao et al. 2008). The other linkage to the erythrocyte membrane by attaching to two self-associating band 3 dimers through the scaffolding protein ankyrin (Bennett and Stenbuck 1979). The band 3-ankyrin complex will be discussed in further detail later.

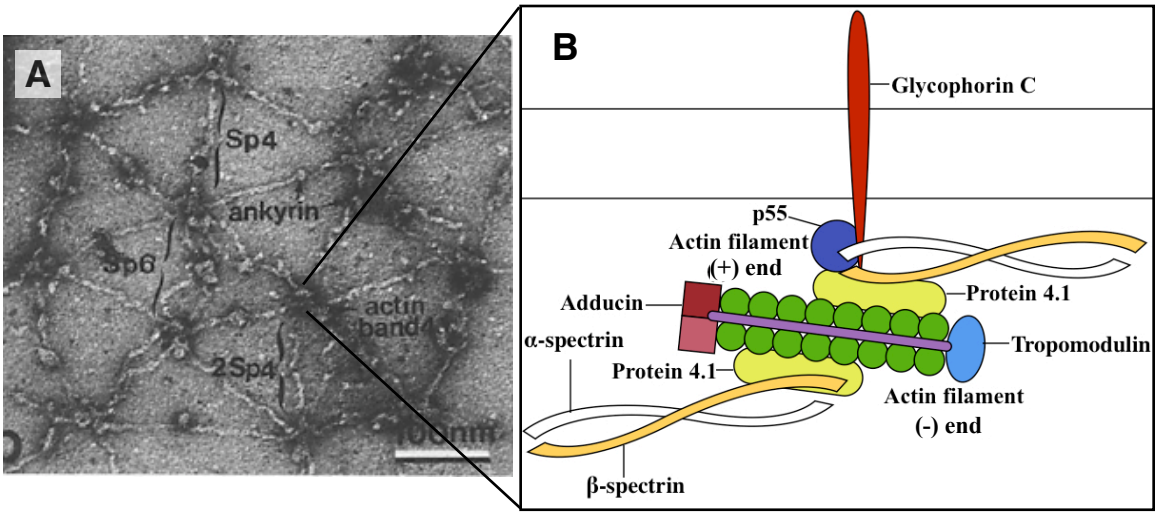

Figure 1. Organization of the erythrocyte membrane cytoskeleton

***A*:** Transmission electron micrograph of the erythrocyte cytoskeleton. Approximately six spectrin tetramers are cross-linked at junctional nodes, forming a hexagonal lattice. (Liu et al. 1987)

***B*:** The spectrin-actin junction. Short F-actin filaments join spectrin at the junctional nodes in *A*. The negative end of the actin filaments are blocked by tropomodulin whereas the positive end interacts with adducin. Nonmuscle tropomyosin lies along the length of the actin filaments. Protein 4.1 induces the spectrin-actin interaction and forms a complex with p55 and the transmembrane protein glycophorin C.

Mechanical Properties of the Erythrocyte Cytoskeleton

The main purpose of the red blood cell cytoskeleton is to maintain the cell's characteristic biconcave shape, a shape that allows the cell to undergo major shape deformations in order to pass through capillaries without fragmenting. Due to these requirements, the erythrocyte membrane must be both highly deformable and extremely stable. Studies of pathologically and biochemically perturbed erythrocyte membranes has shown that deformability and stability of the membrane are regulated independently by separate cytoskeletal components (Chasis and Mohandas 1986). Spectrin's structure plays an important role in maintaining this flexibility. Spectrin is comprised of 106 amino acid triple helical segments that are connected to adjacent segments via short nonhelical regions (Speicher and Marchesi 1984). The folded stability of these repeats varies along the length of the protein and, together with the hinge region created by the linker, provides spectrin with flexibility along its length (MacDonald and Cummings 2004). Atomic force microscopy-related techniques have also shown the unfolding forces of the α-helical repeats to be much lower than domains containing β-folds, with the unfolding process being cooperative in consecutive repeats (Rief et al. 1999; Law et al. 2003).

Aside from the intrinsic properties of the proteins, a number of outside factors effect the mechanical properties of the red cell membrane. The rigidity of the cell during its deformation is influenced by intracellular calcium concentrations (Brody et al. 1995). Calcium is known to interact with the spectrin-protein 4.1-actin complex as well as the spectrin-ankyrin-band 3 complex, inducing decreased deformability (Takakuwa and Mohandas 1988, Liu et al. 2005). The study

of membrane abnormalities has shown that the bridging of the cytoskeleton to the lipid bilayer through ankyrin also plays a role in membrane stability. While not as pronounced as with spectrin disorders, abnormalities in ankyrin reduce the membrane shear elasticity of red blood cells (Waugh 1987).

Erythrocyte Cytoskeleton Disorders

Hemolytic anemia is a state of increased red blood cell destruction. The disorders of the red blood cell membrane that result in hemolytic anemia are predominantly hereditary in nature, though a few acquired defects exist. A number of genetic mutations are associated with hereditary spherocytosis (HS) and will be discussed later. Hereditary elliptocytosis (HE) and hereditary poikilocytosis (HP) are two forms of the same disorder that only differ in their severity with HP being the more symptomatic of the two. A majority of the mutations leading to HE/HP are found in spectrin, with all spectrin mutations lying at or near the self-association site of the α- and β-spectrin chains (Maillet et al. 1996). Southeast Asia Ovalocytosis (SAO) is a symptomless disorder that occurs in people from Papau New Guinea, the Philippines, and other neighboring countries. The mutation responsible results in a gap of nine amino acids at the juncture between the transmembrane and cytoplasmic domains of band 3 (Jarolim et al. 1991).

Structure and Function of Anion Exchanger 1

Topology and Function of AE1 Transmembrane Domain

AE1, also known as band 3, is the prototypical member of the SLC4 gene family, a family of three Cl^-/HCO_3^- anion exchangers. The mechanism of anion exchange has been studied using disulfonic stilbene derivatives since they inhibit anion permeability while having no effect on cations. One of the more potent disulfonic stilbenes, DIDS, was used to identify band 3 as the mediator of anion exchange (Cabantchik and Rothstein 1974). An analogue of DIDS, H_2DIDS, was later used to support the ping-pong model for one-to-one exchange of anions across the plasma membrane by confirming the existence of two conformations dependent on the chloride concentration across the membrane. In this model, there is only one transport site that can face either the intracellular or extracellular space. When intracellular chloride is increased in the presence of a constant extracellular chloride concentration, more of the anion binding sites face outward, detectable by an increase in H_2DIDS inhibition (Furuya et al. 1984).

The transmembrane domain of band 3 (tdb3) is the domain responsible for this physiological function. Located at the C-terminal end of band 3, tdb3 is believed to contain 12-14 transmembrane regions (Figure 2) (Zhu et al. 2003). Further studies have been performed to develop a model of how the transmembrane segments are organized relative to the dimer interface (Groves and Tanner 1999).

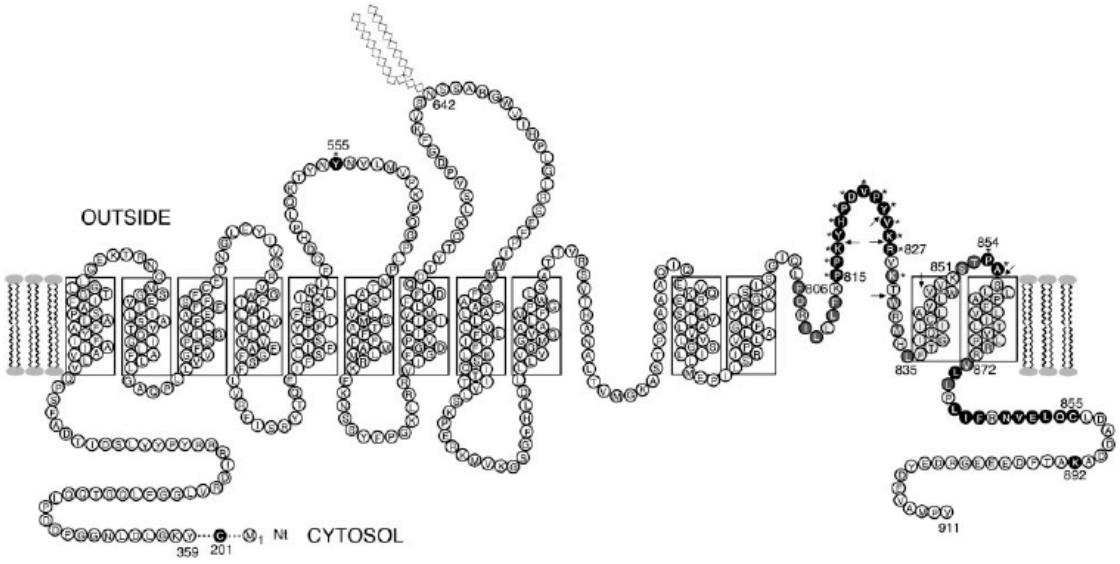

Figure 2. Proposed topology of AE1 transmembrane domain

Putative topology of the AE1 transmembrane domain determined using cysteine-scanning mutagenesis and sulphhydryl specific chemistry. Arrows indicate proteolytic sites, the shading indicates the degree of biotin maleimide labeling, and an asterisk indicates a cysteine mutant was accessible to qBBR, showing that site to be exposed to the extracellular medium. This model displays thirteen transmembrane segments with another possible transmembrane segment between the ninth and tenth segments. (Zhu et al. 2003)

Structure and Function of AE1 Cytoplasmic Domain

The cytoplasmic domain of band 3 (cdb3) serves as a major organization center for the red blood cell membrane. As an anchoring point, cdb3 interacts with a number of proteins including ankyrin (Bennett and Stenbuck 1980), protein 4.1 (Pasternack et al. 1985), protein 4.2 (Korsgren and Cohen 1988), glyceraldehyde-3-phosphate dehydrogenase (GAPDH) (Beth et al. 1981, Rogalski et al. 1989), phosphofructokinase (PFK) (Jenkins et al. 1985), aldolase (Murthy et al. 1981), hemoglobin (Walder et al. 1984), and hemichromes (Waugh and Low 1985) (Figure 3). Band 3 is also a substrate of the protein tyrosine kinase p72syk (Harrison et al. 1994).

Through these interactions band 3 is involved in many processes within the red blood cell, most notable of which is its role in the mechanical properties of the erythrocyte membrane. Band 3 is connected to the spectrin cytoskeleton in two separate macromolecular complexes (Salomao et al. 2008). The complex involving protein 4.1 has been described previously. The second complex involving ankyrin and protein 4.2 (Su et al. 2006) is the principle bridge between the erythrocyte cytoskeleton and the lipid bilayer. The interaction between ankyrin and cdb3 is essential for the morphology and stability of the red blood cell membrane (Low et al. 1991; Peters et al. 1996; Anong et al. 2006) and protein 4.2 may help stabilize this interaction (Rybicki et al. 1988). The cytoplasmic domain of band 3 also has shown a role in membrane deformability both through its interaction with the cytoskeleton and its own inherent flexibility (Mohandas et al. 1992; Uyesaka et al. 1992; Blackman et al. 2001). Cdb3 plays an inhibitory role in glycolysis through its interaction GAPDH, PFK, aldolase, and hemoglobin. (Low et al. 1993; Weber et al. 2004; Campanella et al. 2005). In addition to these interactions, the anion exchanger activity of band 3 is modulated by the binding of factors such as hemoglobin and magnesium to cdb3 (Galtieri et al. 2002; Teti et al. 2002).

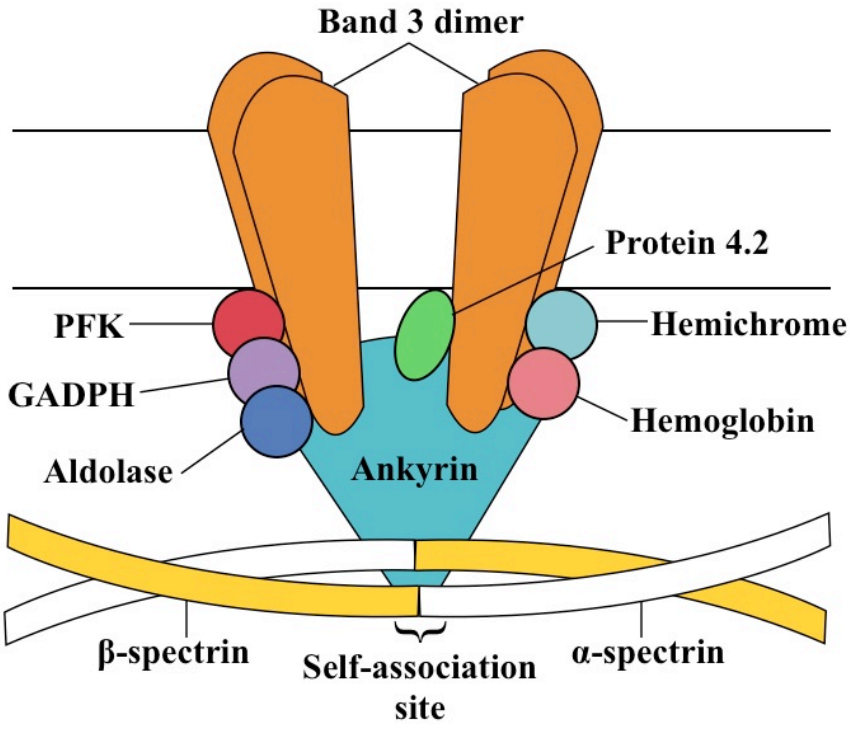

Figure 3. Erythrocyte membrane-cytoskeleton connection

Ankyrin interacts with β-spectrin at the spectrin self-association site. Each ankyrin is capable of cross-linking two band 3 dimers. The association of ankyrin with band 3 is stabilized by protein 4.2. The cytoplasmic domain of band 3 also complexes with phosphofructokinase (PFK), glyceraldehyde-3-phosphate dehydrogenase (GAPDH), aldolase, hemichrome, and hemoglobin at this junction.

Structural studies of cdb3 have revealed a compact symmetric dimer with N- and C-terminal tails lacking secondary structure (Figure 4A). Each monomer contains 11 β-strands and 10 α-helices. Eight of the β-strands form into a β-sheet consisting of both parallel and antiparallel strands. Along with the first six helices, this central β-sheet makes up the central globular domain of the cdb3 monomer. Two of the remaining β-strands spanning residues 175-185 form a β-hairpin loop while the last β-strand is part of the dimerization arm. The dimerization arm is a largely helical segment at the C-terminal end of cdb3 and is connected to the globular domain by a short helix and loop segment (Figure 4B) (Zhang et al. 2000; Zhou et al. 2005). Loss of the β-hairpin loop makes a mutant that is has no affinity to ankyrin, identifying this loop as necessary for the interaction with ankyrin (Chang and Low 2003). This segment alone, however, is not sufficient for the binding of ankyrin. Antibodies developed against residues 118-162 of cdb3 also inhibited the binding of ankyrin (Davis et al. 1989). A computational model of the cdb3-ankyrin complex has identified further areas possibly involved in the binding site with total of over 1,500Å^2 of buried surface area (Michaely et al. 2002).

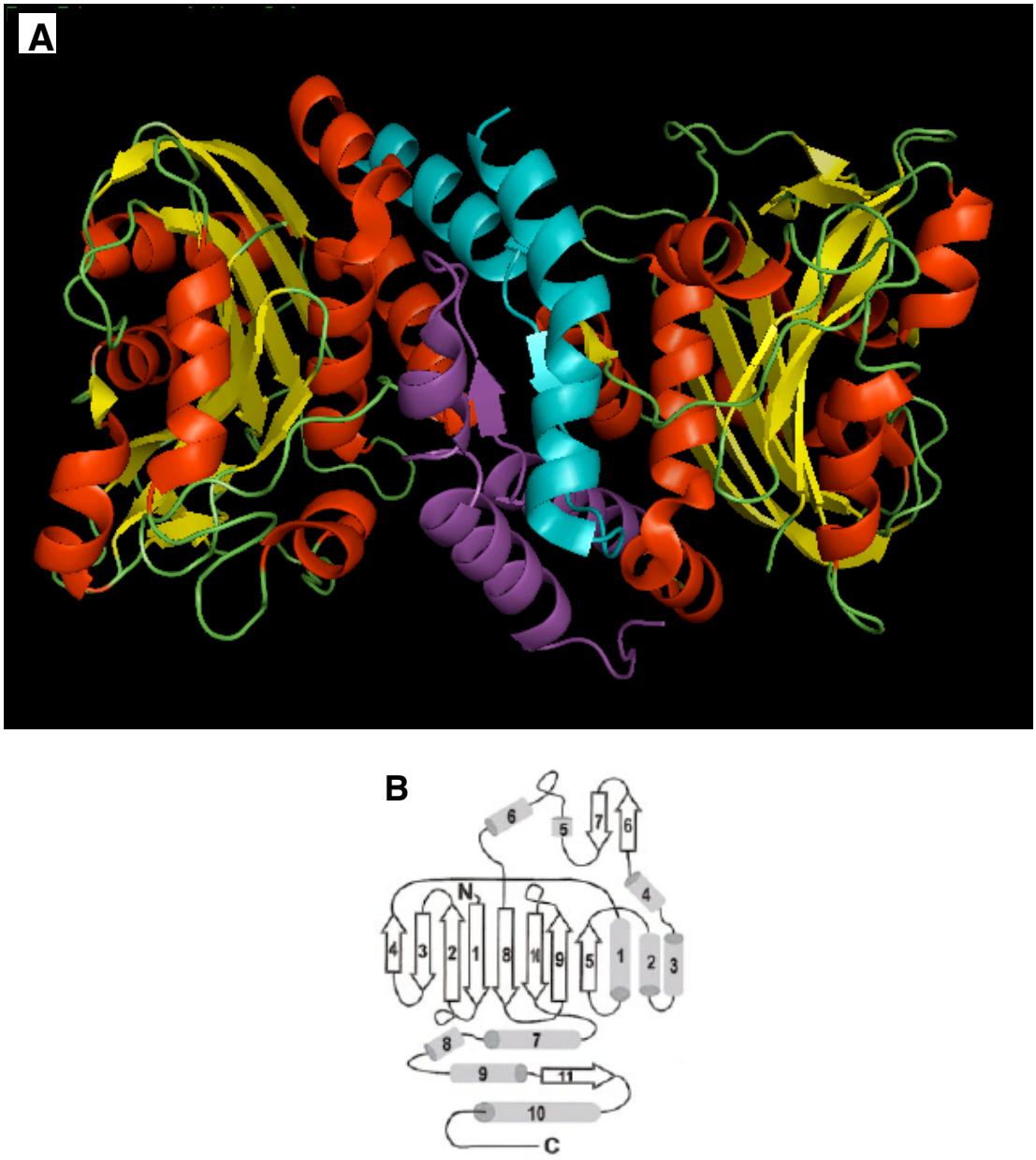

Figure 4. Structure of the cytoplasmic domain of human band 3

***A*:** Crystal structure of cdb3 at pH 4.8. The cdb3 dimer is displayed in ribbon diagram colored based on secondary structure. The dimerization arms (304-357) are highlighted in cyan and purple.

***B*:** Diagram of cdb3 monomer secondary structure. The cdb3 monomer includes 11 β-strands and 10 α-helices. β-strands 1-4, 5, and 8-10 form a central β-sheet containing both parallel and antiparallel strands while β-strands 6 and 7 form a b-hairpin loop. These elements form a globular domain together with the first six helices. The remaining helices and β-strand 11 form the dimerization arm indicated in *A*. (Zhang et al. 2000)

Hereditary Human Spherocytosis

Normal Physiology of the Red Blood Cell

Erythrocytes develop from pluripotent hematopoietic stem cells found in the bone marrow through a process known as erythropoiesis. The first definite erythrocyte precursor is known as a pronormoblast that further develops into the nucleated normoblast. As the normoblast develops it progressively shrinks and the cytoplasm becomes less basophilic and increasingly acidophilic due to the build up of hemoglobin. By the final form of the normoblast, the nucleus is pyknotic and the cell is only about 5 microns in diameter. At this point, the normoblast loses its nucleus and leaves the bone marrow as a reticulocyte. An alteration in the cell shape occurs outside the bone marrow and after one to two days the reticulocyte becomes a mature erythrocyte (Dacie and White 1949). Mature erythrocytes are about 7.5 microns in diameter and 2 microns thick. An erythrocyte will survive around 120 days in circulation before being removed and most of its iron is recycled. Each cell contains high amounts of hemoglobin, making erythrocytes well-suited for the transport of oxygen to tissue throughout the body (Silbernagl and Despopoulos 88).

Due to the lack of organelles and its membrane skeleton, the erythrocyte is very deformable. The nature of blood is such that its viscosity when passing through small arteries is about 4 relative units, twice as high as that of plasma. This viscosity increases in smaller vessels since the velocity of flow decreases, but red blood cells compensate by traversing capillaries in single file. The deformable nature of their membranes allows them to pass through safely despite the smaller

diameter of the capillaries (92) In capillaries closer to the diameter of the erythrocyte, the cell takes on a parachute-like shape (Figure 5A). In narrow capillaries around 4 microns in diameter, the most common shape is a torpedo shape (Figure 5B) (Skalak and Branemark 1969).

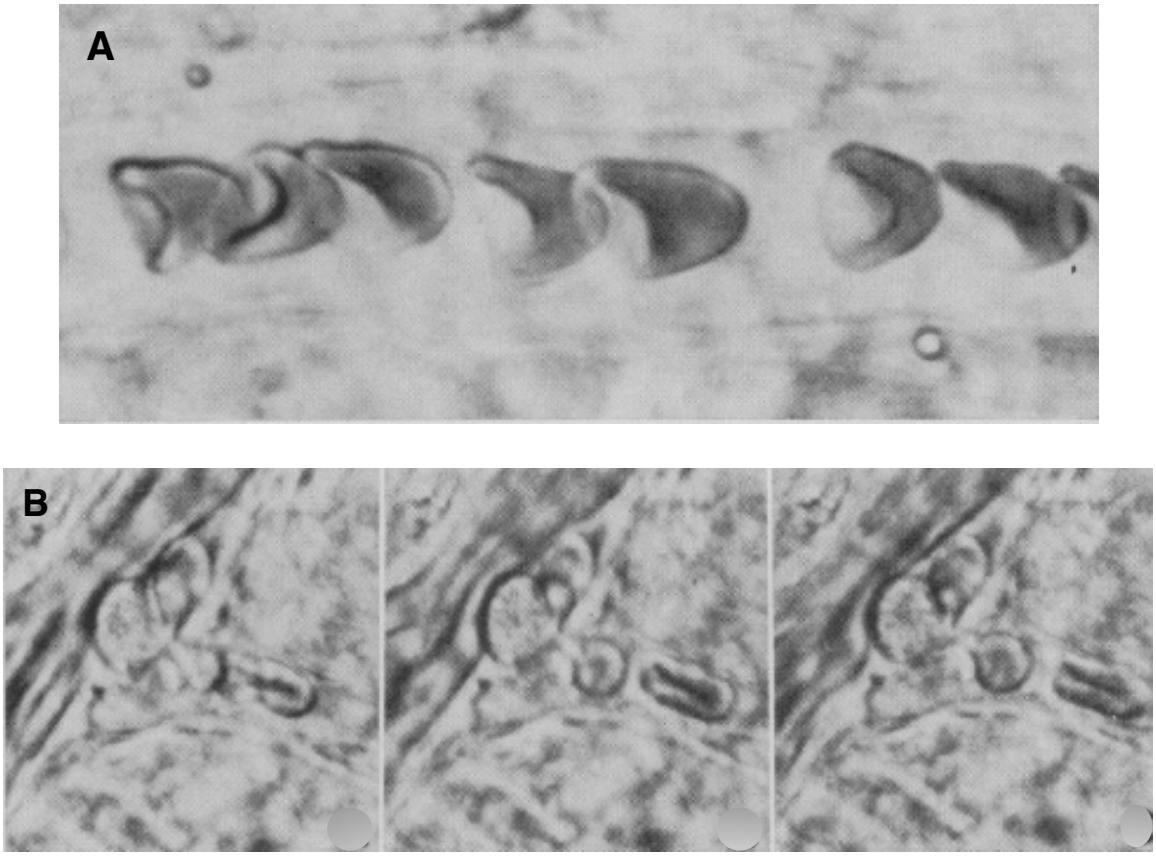

Figure 5. Deformation of red blood cells

***A*:** The parachute shape of *In vivo* erythrocytes traversing a 7 μm capillary with the cell on the left displaying the tail-flap appearance.

***B*:** Red blood cells passing through 4 μm capillary adopt a U-shape or hollow torpedo shape.

Pathophysiology of Hereditary Spherocytosis

Hereditary Spherocytosis (HS) refers to a group of inherited hemolytic anemias associated with defects in the erythrocyte membrane skeleton. The prevalence of HS is highest in northern Europe and North America, affecting about one in every 2000 people. Three fourths of HS cases display an autosomal dominant inheritance pattern while the remaining cases have a more severe autosomal recessive form. HS results from mutations affecting the proteins involved in the spectrin-ankyrin-band 3 complex. Mutations in the ANK1 gene for ankyrin make up 50% of the autosomal dominant cases of HS while another 15-20% of cases are due to a mutations in SLCA1, the gene for band 3. Other mutations that result in HS can be found in SPTA1, SPTB, and EPB42, the genes that encode for α-spectrin, β-spectrin, and protein 4.2, respectively (Delaunay 2002). All of these mutations cause a disruption in the link between the erythrocyte cytoskeleton and the membrane, resulting in reduced membrane surface area, a decreased membrane to surface ratio, and the formation of spherocytes to compensate for these changes (Figure 6). These spherocytes end up trapped in the spleen where low pH, low glucose and adenosine triphosphate concentrations, contact with macrophages, and high local concentrations of oxidants deliver additional damage. The destruction of abnormal erythrocytes by the spleen is the main cause of hemolysis in HS (Perrotta et al. 2008)

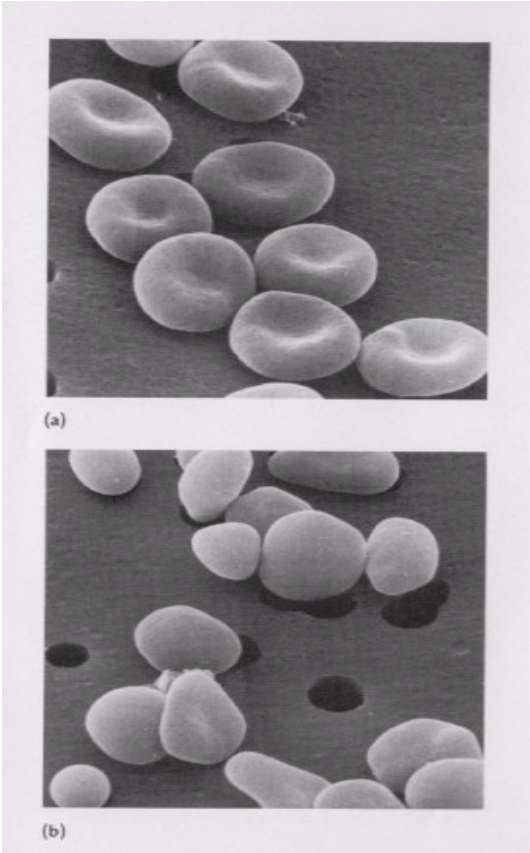

Figure 6. Scanning electron micrograph of red blood cells

(a): The normal biconcave shape of erythrocytes.
(b): Erythrocytes from a HS patient have spherical shape and smaller cell size. (Agre et al. 1982)

Complications and Therapies of HS

Patients with HS can present with various symptoms such as anemia, splenomegaly, and jaundice. HS is diagnosed based on the presence of spherocytes in peripheral blood smears, increased osmotic fragility, and a positive family history. The severity of the disease varies from individual to individual with 20-30% of patients remaining asymptomatic due to compensation by increased erythropoiesis. In most cases, the compensatory measures taken by the body to match red cell destruction are outpaced, leading to chronic hemolysis (Kumar, Abbas, and Fausto

644). This state leads to the formation of bilirubinate gallstones, which are the most common complication of HS. Gallstones are found in 40-50% of patients in their second to fifth decade with a majority of cases in those between 10 to 30 years of age. Co-inheritance of Gilbert's Syndrome, the most common hereditary cause of increased bilirubin, increases the risk of developing cholelithiasis up to five-fold. Timely diagnosis, best done by ultrasonography, allows for quick treatment to stem the possibility of biliary tract diseases like cholecystitis and cholagnitis.

Most patients also experience a few anemic crises in their lifetime. Hemolytic crises are produced by events that lead to increased splenic destruction of red blood cells, as in the case of Epstein-Barr virus infection. Cases are typically mild and punctuated by transient jaundice, splenomegaly, reticulocytosis, and anemia. Aplastic crises are less common and are triggered by acute parvovirus infection. Parvovirus infects the bone marrow, killing red cell progenitors and stopping red cell production for 1-2 weeks until an immune response is mounted. Aplastic crises lead to severe anemia that requires in-hospital treatment and transfusion, and patients may face complications as serious as congestive heart failure or death. Megaloblastic crises are rare and typically only found in underdeveloped countries where nutrition is an issue. Since these cases are caused by folate deficiency, they can occur in patients with increased folate demand (e.g. pregnant women, children, and patients recovering from an aplastic crisis) and can be treated with folate supplements. Rarely in cases of severe HS, patients can develop other manifestations such as leg ulcers, gout, chronic dermatitis, extramedullary hematopoietic

tumors, hematological malignant diseases (e.g. multiple myeloma and leukemia, and angioid streaks).

Splenectomy is often beneficial to most patients with the treatment eliminating the anemia and hyperbilirubinemia and reducing reticulocyte counts to near-normal levels. Splenectomy does involve risk and a serious long-term complication is overwhelming infection with encapsulated bacteria, usually *Streptococcus pneumoniae*. In some regions of the world, fulminant parasitic infections can occur. Immunization, prophylactic use of penicillin, or early antibiotic treatment can help reduce, but not eliminate, the incidence of postsplenectomy infection. Splenectomy is recommended between ages 6-9, as the risk of infection is higher in young children and the risk of cholelithiasis is higher in children over 10 years old. An alternative to total splenectomy is partial splenectomy. Partial splenectomy removes enough spleen to reverse anemia and relieve symptomatic splenomegaly while still preserving the immune function of the organ (Perotta et al. 2008). A laparoscopic approach to the procedure has been developed and a clinical study has been done to compare the outcome of a group of patients who underwent that procedure to patients who underwent laparoscopic total splenectomy. Laparoscopic partial splenectomy is associated with more pain, longer oral intake time, and a longer hospital stay than laparoscopic total splenectomy, but retained splenic function may outweigh these short-term disadvantages. Long-term results of patient outcome have yet to be reported for this more recent therapy (Morinis et al. 2008). Other alternatives include near-total splenectomy and partial splenic embolization, both of which prove safe and effective for the treatment of HS (Stoehr et al. 2005; Kimura et al. 2003).

CHAPTER II

ELECTRON PARAMAGNETIC RESONANCE

Basic Principles of EPR

Origin of the EPR Signal

Every electron possesses a magnetic moment, u, and an intrinsic spin angular momentum with a primary quantum spin number S (S = ½) and a secondary magnetic component M_S (M_S = -½. ½). Due its magnetic moment, an electron will align itself either parallel (M_S = -½) or antiparallel (M_S = ½) in the presence of an external magnetic field with strength B. These two states each have specific energies, known as the Zeeman effect, with the parallel alignment corresponding to the lower energy state and the antiparallel alignment corresponding to the higher energy state. If the direction is chosen to be along B, the two allowed energy states are:

$$E = -\mu_z B = g_e \beta_e M_s B = \pm \frac{1}{2} g_e \beta_e B$$

where g_e is the Zeeman (correction) factor for the free electron g_e = 2.00232 and β_e is the Bohr magneton, which is a physical constant of the electronic magnetic moment

$$\beta_e = \frac{|e|\hbar}{2m_e} = 9.2740154(31) \times 10^{-24} JT^{-1}$$

Unpaired electrons can move between the two electronic Zeeman levels by absorption or emission of electromagnetic radiation of energy *hν* if that energy matches the separation of ΔE, giving the fundamental resonance equation:

$$\Delta E = h\nu = g_e \beta_e B$$

In addition to the external magnetic field, an unpaired electron is affected by the nearby nuclei of atoms, which have magnetic dipole moments that generate a local magnetic field . In EPR, the interaction between these species is called nuclear hyperfine interaction. For a spin label, the unpaired electron (S = ½) interacts with the nitrogen nucleus ^{14}N, which has a primary quantum number I (I=1) and a secondary quantum number M_I (M_I = -1, 0, +1). In this case, the selection rules for EPR absorption ($\Delta M_S = \pm 1$ and $\Delta M_I = 0$) allow for three transition (Figure 7).

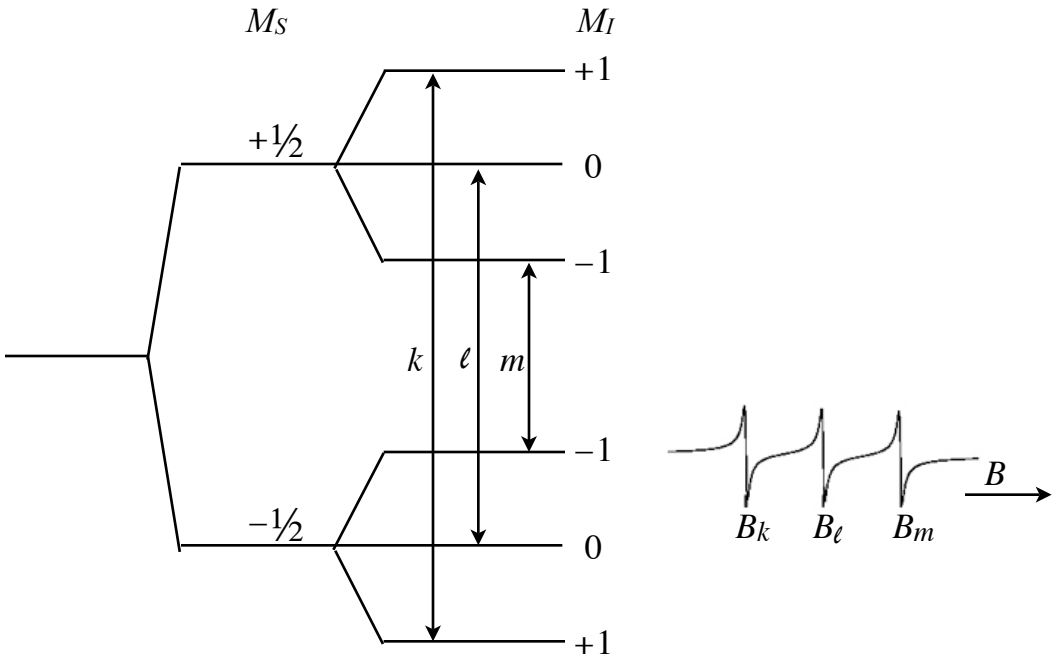

Figure 7. Energy levels of system with S = ½ and I =1

Energy levels and allowed EPR transitions at constant field for a system with S = ½ and I = 1. Energy levels are represented with horizontal lines marked with M_S and M_I values. The allowed EPR transitions are indicated by the vertical arrows labeled k, l, and m. A simulated EPR field sweep spectrum depicting these transitions is shown on the right.

Two unpaired electrons in close proximity to each other interact either by orbital overlap, known as electron exchange interactions, or through space, known as electron-electron dipole interactions. For example, if the electron orbitals of two unpaired electrons overlap in a paramagnetic center of moderate size, the system will separate into a triplet (S = 1) and a singlet (S = 0) state. The electron-electron dipole interaction behaves like anisotropic hyperfine interaction between electronic and nuclear magnetic dipoles.

As with NMR, two relaxation processes exist in EPR. T_1, the spin-lattice relaxation time, describes the time required for the redistribution of spin-orientation states back to thermal equilibrium. Other relaxation processes such as spin diffusion are characterized by T_2, the spin-spin relaxation time. These processes have the effect of varying the relative energies of the spin levels rather than their lifetimes. For nitroxides, T_2 is in the 100-nanosecond range while T_1 is normally in the microsecond range at ambient temperature.

Spin Dynamics

EPR lineshapes can be affected by any dynamic process in or around the paramagnetic center, such as hindered rotation, molecular tumbling, and chemical reaction. Lineshape broadening can classified as homogeneous or inhomogeneous broadening. Homogeneous broadening arises from a set of equivalent spins with identical spin parameters and local fields. Spin lifetime (T_1), spin diffusion (T_2), and dynamic processes contribute to homogeneous linewidth. Inhomogeneous broadening from nonequivalent spins is due to the variation of the external magnetic field and unresolved hyperfine structure.

Conventional EPR operates in the 1 to 100 GHz frequency range, making it sensitive dynamics on the nanosecond time scale. Fast motions of less than 1 ns, such as side chain motions of surface residues, give rise to sharp spectra. Intermediate motions of 1 to 10 ns, such as the backbone motions of surface exposed loops, lead to homogeneously broadened spectral features. Slow motions of 10 ns to 1 μs, such as the global tumbling of large globular proteins in solution, leads to the spectral features of the anisotropic magnetic interactions. Rigid motions that correspond to certain conformational changes and global uniaxial rotations of transmembrane proteins within the lipid bilayer result in powder specter in continuous wave EPR (CW-EPR) (Hustedt and Beth 1999). In biological systems, molecular motions can range from 10-14 s (bond vibration) to 10 s (local denaturation). Saturation transfer EPR (ST-EPR) spectroscopy can be used for the slower motions to the ms time scale. In ST-EPR, one narrow region of the inhomogeneously broadened EPR signal is saturated. The recovery and spreading of the saturation via spin diffusion is studied by monitoring secondary harmonic signals.

Pulsed EPR

To help understand the complicated motions of a sample, it is advantageous to use a rotating coordinate system referred to as the rotating frame (Figure 8). In the presence of an external field, B, each electron spin magnetic moment undergoes precession around the z direction at its Larmor frequency, ω_B. In the EPR experiment, circularly polarized B_1 with a microwave frequency of ω is applied perpendicular to B, with $\omega_B = \omega$ at resonance. In a rotating coordinate system with angular frequency ω, B_1 appears stationary along the x-axis and the Larmor pre-

cession around the z-axis is no longer visualized. The bulk magnetization, M, rotates about the x-axis and is tilted into the xy-plane at the tip angle $\alpha = |\gamma_e B_1| t_p$, where γ_e is the gyromagnetic ratio of an electron and t_p is the length of time B_1 is applied. In CW-EPR, where B_1 maintains a constant amplitude with time, the spins are driven back and forth between states $M_S = \pm ½$. Given an adequate T_1 relaxation process, a population difference is maintained and a net absorption signal is observed. In pulsed EPR, where t_p is on the order of several nanoseconds, the excitation amplitude is time dependent. Pulses are often labeled by their tip angles, for example a $\pi/2$ pulse corresponds to a rotation of M_0 by $\pi/2$. Combining different pulses at different times can generate a plenitude of information regarding a spin system. Well developed pulsed techniques include electron spin echo envelope modulation (ESEEM) and double electron electron resonance (DEER) also known as pulsed ELDOR (electron electron resonance).

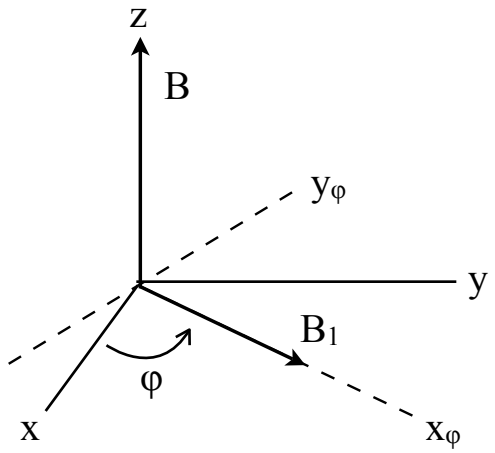

Figure 8. Rotating frame in relation to lab frame

The Cartesian coordinates (xyz) represent the lab frame. The static magnetic field **B** lies along the z-axis. The oscillating magnetic field $\mathbf{B_1}$, perpendicular to **B**, rotates around the z-axis (azimuthal angle φ) in the xy-plane at the angular frequency ω. The rotating frame ($x_\varphi y_\varphi z$) also rotates at frequency ω. The x_φ-axis aligns with $\mathbf{B_1}$.

Applications of SDSL in EPR

Site-Directed Spin Labeling

Spin labels, unlike free radicals, are chemically stable and thus useful in EPR experiments. One such agent, methanethiosulfonate spin label (MTSSL), is a pyrroline derivative with four methyl groups to protect the unpaired electron in the pn orbital of the nitroxide (Figure 9). Without these methyl groups, the nitroxides can be easily reduced to hydroxylamine in the presence of a reducing agent such as ascorbic acid. Nitroxides can be covalently bound to a number of agents ranging from small molecules to certain components of macromolecules. In the case of site-directed spin labeling with MTSSL, the nitroxide binds to free cysteine residues.

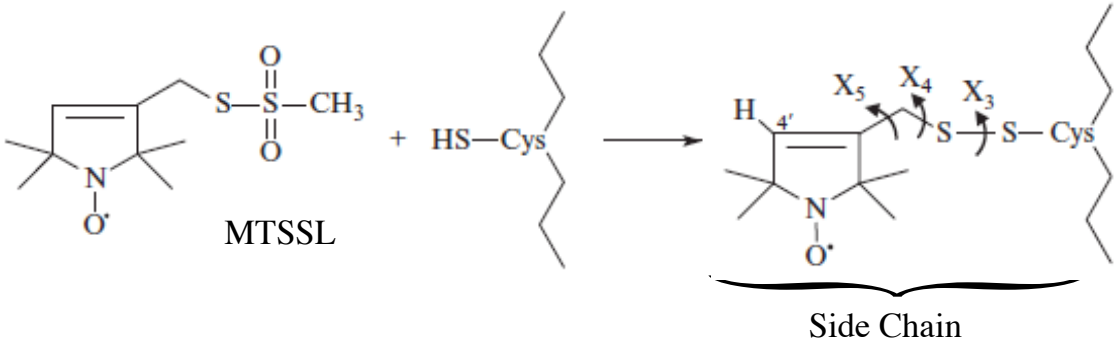

Figure 9. The reaction of MTSSL with cysteine

The unsaturated spin label reacts with a free cysteine residue on a protein to generate the nitroxide side chain R1. Bond rotation angles χ3, χ4, and χ5 that relate the spin label to the cysteine residue are defined. (Klug and Feix 2008)

The basic strategy of SDSL benefitted greatly from the development of molecular cloning and site-directed mutagenesis. The technique requires the substitution of all the native nondisulfide bonded cysteine residues with either alanines or serines and then reintroducing a single cysteine mutation at the site of interest. The reactive SH group can then be modified by the introduction of a nitroxide spin label. The commercially available ethanethiosulfonate derivatives, such as MTSSL, are widely use to generate disulfide linked nitroxide side chains. There is much evidence to support that the introduction of these single cysteine mutations and spin labeling have minimal effect on the structure and function of the protein. The pairing of SDSL with EPR can provide previously unavailable information since it is not limited by protein size nor by the optical properties of the sample. This technique is a versatile approach to providing local and global structural information.

Side Chain Mobility

The simplest information that can be obtained from an EPR spectrum concerns spin label motion since the lineshape itself reflects rotational mobility. X-band CW-EPR is sensitive to motions in the nanosecond time scale. The dynamics of free spin label is described by the rotational correlation time τ. With nitroxides, τ measures the average lifetime of a particular spatial orientation of the nitrogen p orbital and its reciprocal is the rate of motion of the spin label (Columbus and Hubbell 2002). EPR lineshapes thus reflect the rotational motions of different correlation times (Figure 10). Free spin label in solution experiences a fast correlation time (~0.1 ns) and the resulting EPR spectra contains three sharp lines of ap-

proximately equal height. As the motion of the side chain is slowed and the correlation time lengthens, the peaks on the EPR spectra broaden. Since the signal intensity is proportional to the amplitude and the square of the linewidth, the amplitude decreases as the lines broaden.

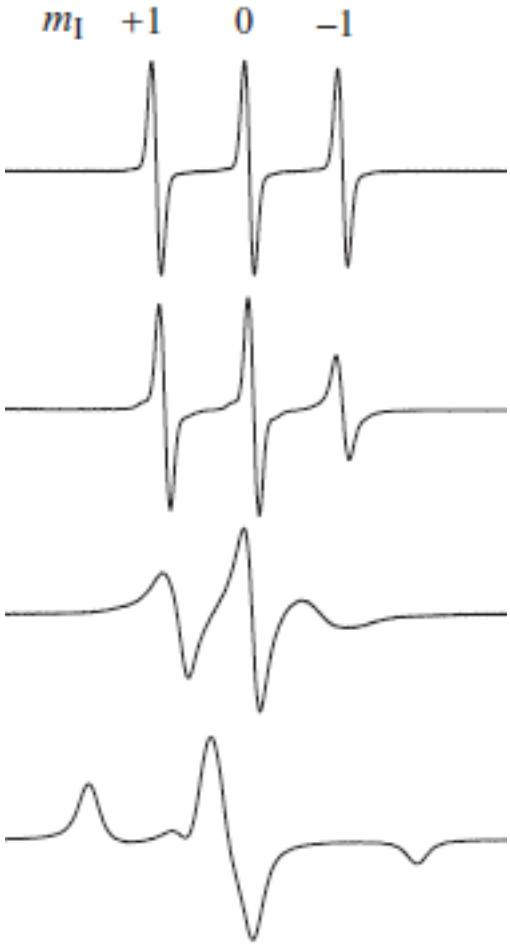

Figure 10. The relation of correlation time and CW-EPR lineshapes

Simulated X-band CW-EPR lineshapes of a nitroxide spin label at different correlation times. The changes in EPR lineshape reflect changes in the rotational motion of the sample. The first derivative spectrum of the fast rotational motion ($\tau \rightarrow 0$) displays three sharp lines. As the rate of motion decreases and the correlation time increases, the spectrum broadens and becomes more complex. At the rigid limit ($\tau = \infty$) the powder spectrum can be observed in a system of random oriented single crystals, where each experiences highly anisotropic motion. (Klug and Feix 2008)

When the spin label is attached to a protein backbone, the side chain will be affected by the rotational diffusion of the protein, internal dynamic modes of the side chain, tertiary interactions with nearby moieties, and local backbone structure. For larger proteins and macromolecular assemblies, the overall rotation is too slow to affect the EPR spectra. The tumbling of small proteins (> ~15kDa), however, can affect the spectra. This contribution can be reduced by increasing solution viscosity, for example, by adding 30% (w/w) sucrose to the sample (Mchaourab et al. 1996). The side chain motion is the primary interest since it is the motion that is affected by tertiary contacts and the local environment. A number of studies have shown that the flexibility of MTSSL is generally governed by the two bonds closest to the nitroxide ring, χ_4 and χ_5 (Figure 9) (Langen et al. 2000; Columbus et al. 2001). Even on a solvent exposed helix with no adjacent contacts, the hydrogen bond formed between the S_δ sulfur and the backbone C_α atom restricts the mobility about the first two bonds, limiting the internal motion of the R1 side chain to isomerizations around the χ_4/χ_5 dihedral angles (Langen et al. 2000). Therefore the motion of the spin label and the backbone fluctuations are linked.

Tertiary contacts with nearby side chains have more significant effects on EPR spectra. Spin labels with these interactions exhibit complex lineshapes and site buried in the core of a protein often display spectra approaching the rigid limit. Parameters regarding mobility can be attained from components of the spectra, such as the peak-to-peak linewidth and the center linewidth. More detailed quantitative analysis can be performed by simulating the EPR spectrum in order to obtain rotational correlation times and other order parameters.

Solvent Accessibility

The accessibility of the R1 side chain to the solvent provides a good deal of structural information about the protein. Since the power saturation technique utilizes the fact that certain paramagnetic reagents affect the relaxation rate of the spin label, it is a useful tool for studying solvent accessibility. When under nonsaturating conditions, the height of the spectral line increases linearly with the square root of the incident power, $P_{½}$. As the microwave power increases, the sample cannot relax fast enough and the relationship is no longer linear. At even higher power, the height of the spectral line decreases. When certain paramagnetic reagents react with the spin label, the relaxation rate is increased and more power is able to be absorbed before saturation. The two main paramagnetic reagents typically used are O_2, which is mainly found in the hydrophobic portion of the lipid bilayer, and nickel compounds such as nickel(II) ethylenediamine diacetate (NiEDDA), which are water soluble. Nitrogen is used to purge molecular oxygen from the sample as a control.

R1 solvent accessibility is sensitive to the local environment since it has a large influence on the collision frequency between the nitroxide and the paramagnetic reagent. The direct measure of the bimolecular collision rate between the spin label and the paramagnetic reagent is the value $\Delta P_{½}$. $P_{½}$ is the power at which the height of the central linewidth is half of its unsaturated intensity. In the case of NiEDDA, the $P_{½}$ of the N_2 control is subtracted from the $P_{½}$ in the presence of NiEDDA to give $\Delta P_{½}$. For a solvent-exposed residue, a high $\Delta P_{½}$ value would be observed. In addition, secondary structure can be observed for a-helices and b-strands that experience amphipathic environments. An α- helix, for example,

would experience a $\Delta P_{½}$ with a periodicity of 3.6 (Figure 11A) while a β-strand would have an periodicity of 2 (Figure 11B). Since oxygen is lipid-soluble, it can be used together with NiEDDA to study the depth of a residue within the lipid bi-layer. The $\Delta P_{½}$ for the two reagents would be the inverse of one another, with higher $\Delta P_{½}(O_2)$ and lower $\Delta P_{½}$(NiEDDA) indicating a residue found in the hydro-phobic region of the membrane. Changes in O_2 and NiEDDA accessibility can also be reflective of conformational changes. This method has been useful for studying dynamic processes such as light activation of rhodopsin (Farrens et al. 1996) and gating of the mechanosensitive channel MscL (Perozo et al. 2002).

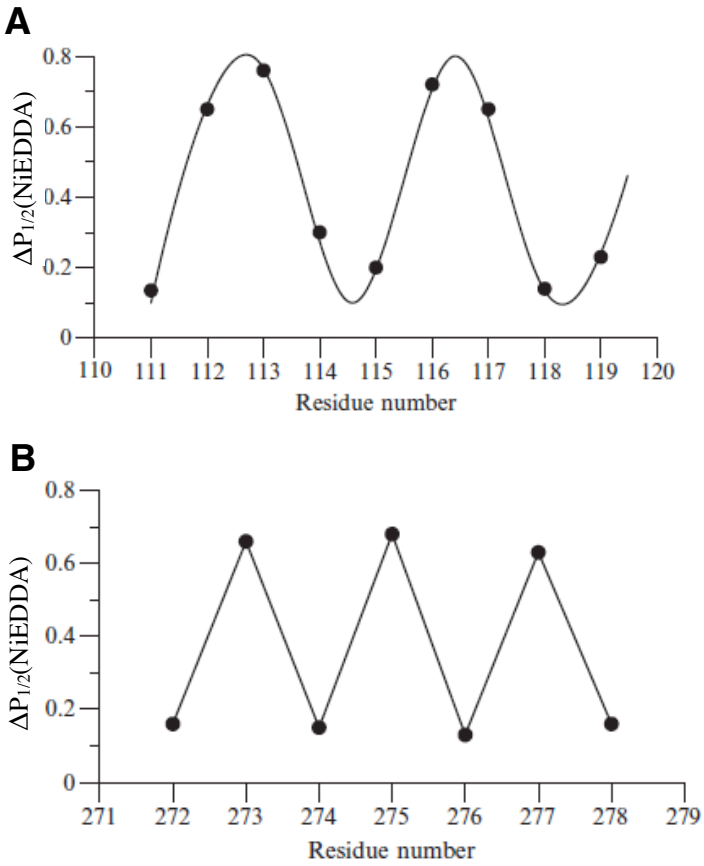

Figure 11. Solvent accessibility of secondary structures

(a): A surface α-helix on a water soluble protein displays a pattern of NiEDDA accessibility that repeats approximately every 4th residue, following the 3.6 residue turn of a typical helix.

(b): The solvent accessibility of a surface β-strand alternates between a high and low $\Delta P_{½}$, indicating solvent-exposed and buried residues, respectively. (Klug and Feix 2008)

Spin-Spin Distance

The ability to make distance measurements between two spin labels is a rapidly developing field of EPR. CW-EPR can make measurements between 8 Å to 25 Å where the spin-spin interactions are larger than the inhomogeneous line broadening. Pulsed EPR techniques can cover distances from 17 Å to 80 Å. These distance measurements can be used for many purposes, such as monitoring con-

formational changes and developing structural models. Distance measurements depend on the dipolar coupling interaction between the unpaired electrons of the two spin labels. In CW-EPR, magnetic dipole interactions result in line broadening and an accompanying decrease in signal amplitude. Quantitative analysis can be performed through a few different approaches (Altenbach et al. 2001; Steinhoff et al. 1997; Hustedt et al. 1997). The resolution of such methods depends on the flexibility of the R1 side chain, with highly immobilized spin labels giving a resolution on the order of 0.1-0.2 Å (Hustedt et al. 1997).

Pulse EPR techniques, like DEER, have a larger distance range that allow for greater applications. Since the dipole interactions at these distances are smaller than the inhomogeneous broadening, three strategies have been implemented to separate the dipole interactions. The first method involves refocusing all interactions of an observer spin with a second unpaired electron in an echo experiment. The dipolar coupling is then reintroduced by an inversion pulse applied to the second spin. The second method is to observe the double quantum coherence caused by the coupling of the two spins. The third method is to refocus all interactions except the coupling using a solid echo. These methods provide the modulations between the electron spins that can be analyzed to determine the distance between two labels.

CHAPTER III

GENERAL EXPERIMENTAL METHODS

CW-EPR Measurements

X-band (9.8 GHz) CW-EPR spectra were collected using a Bruker EMX spectrometer equipped with a TM_{110} cavity (BrukerBiospin, Billerica, MA) at room temperature. Samples were drawn into 50 μL glass capillaries (VWR, West Chester, PA) and sealed with Critoseal sealant (Fisher, Pittsburgh, PA).

Solvent Accessibility

Solvent accessibility of individual spin-labeled residues was measured on samples diluted to 100 μM spin concentration in 20 nM NaH_2PO_4, 100 mM NaCl, pH 6.8. NiEDDA was added to a final concentration of 5 mM. Samples were purged of molecular oxygen by flowing nitrogen gas over the sample contained in a TPX capillary for 20 minutes prior to and during measurements. An ER4123D dielectric resonator was utilized for collection. A 20 Gauss scan of the central resonance line for each mutant was carried out using a 1 Gauss modulation amplitude of 100 kHz frequency. A total of 24 scans were separately recorded at microwave powers ranging from 1 mW to 200 mW using a 1dB attenuation per step. Data were analyzed using Origin 6.1 software (OriginLab Corporation, Northampton, MA) by a non-linear least squares curve fitting of the spectral amplitude (A_0) versus the square root of microwave power (P_0) using the equation:

$$A_0 = \frac{c\Lambda\sqrt{P_0}}{[1 + (2^{1/\epsilon} - 1)P_0/P_{1/2}]^{\epsilon}}$$

where A_0 is the peak-to-peak amplitude of the first derivative spectrum, c is the instrumental proportionality constant, LAMBDA is the instrumental factor, P_0 is the input power, ε is the lineshape adjustment parameter, and $P_{½}$ is the half saturation power. The NiEDDA accessibility was calculated by the following equation:

$$Ac(NiEDDA) = \frac{P_{1/2}(NiEDDA) - P_{1/2}(N_2)}{\Delta H_0}$$

where Ac is the accessibility, $P_{½}$(NiEDDA) is the half saturation power in the presence of 5 mM NiEDDA, $P_{½}(N_2)$ is the half saturation power in the absence of NiEDDA, and ΔH_0 is the central line width (Subczynski and Hyde 1981; Altenbach et al. 1989).

CHAPTER IV

STRUCTURE OF CDB3 HEREDITARY SPHEROCYTOSIS VARIANT G130R: BAND 3 FUKUOKA

Introduction

Hereditary spherocytosis (HS) is familial hemolytic disorder clinically characterized by anemia, jaundice, and splenomegaly (See HS section for details). HS occurs in about 1 in every 2000 people. In HS, weakened "vertical" interactions of the cytoskeleton result in membrane blebbing, leading to a decreased surface area-to-volume and the cell becomes spherical. Spherocytes are less deformable and have increased osmotic fragility. These cells are unable to pass through the narrow cords of the spleen where they are removed from circulation and destroyed, resulting in hemolytic anemia. Mutations causing to HS have been identified in the genes ANK1, SLCA1, SPTA1, SPTB, and EPB42 that encode for the proteins ankyrin, band 3, α-spectrin, β-spectrin, and protein 4.2, respectively. Mutations in band 3 make up 15-20% of cases of HS.

Band 3, also known as anion exchanger 1 (AE1), is one of three members of CL-/H3CO- anion exchangers. Band 3 has two functionally distinct domains, a transmembrane and cytoplasmic domain. The transmembrane domain of band 3 (tdb3) makes up the C-terminal end of the protein is responsible for the transport of anions across the erythrocyte membrane. The N-terminal cytoplasmic domain of band 3 (cdb3) serves as an organization center for a number of cytoplasmic and membrane-associated proteins at the lipid bilayer (Lux et al. 1989).

Numerous band 3 mutations have been identified in patients with HS. A study of patients with HS showed that patients with frameshift and nonsense mutations lacked band 3 mRNA in their reticulocytes, leading to an overall decrease in band 3 expression. Point mutations, on the other hand, displayed comparable levels of normal and mutant band 3 (Jarolim et al. 1996). Many point mutations in the transmembrane domain of band 3 have been shown to lead to defective trafficking of the protein to the erythrocyte membrane (Dhermy et al. 1999; Quilty and Reithmeier 2000; Toye et al. 2008). In the cytoplasmic domain of band 3, three mutations have been identified in association with HS. These mutants (E40K, G130R, and P327R) still form dimers at the erythrocyte membrane and have no significant changes in stability, suggesting the mutations interfere with the binding of cdb3 to ankyrin or protein 4.2 (Bustos and Reithmeier 2006). Indeed, past studies have linked the P327R mutation to decreased protein 4.2 binding at the erythrocyte membrane (Jarolim et al. 1992). To better understand the mode of this disruption, site-directed spin labeling was used in conjunction with electron paramagnetic resonance and double electron-electron resonance in order to study the structural changes in the P327R mutant. While the P327R mutation does not disrupt the dimer, it does alter the packing of the C-terminal end of helix 10 in the dimerization arm and elicit spectral changes in the N-terminal portion of helix 10 and some residues in β-strand 11. These results, taken together with previous studies, indicate a potential site for interaction between protein 4.2 and cdb3 (Zhou et al. 2007).

Of the remaining two mutants, E40K is located at the unresolved N-terminus of cdb3 while G130R is located on the surface at the start of helix 2. The

G130R mutant provides an interesting target for the study of structural changes and protein-protein interactions. Clinically, G130R results in a mild form of HS with only a 9.3% reduction in band 3 content in the red blood cell. The protein 4.2 deficiency was more substantial with the protein 4.2 levels at 45% that of normal cells (Inoue et al. 1998). To examine the structural changes caused by this mutation, site-directed spin labeling (SDSL) studies using a combination of CW-EPR and power saturation experiments were conducted on a cysteineless cdb3 background with or without the G130R mutation. In this chapter, data shows that substitution of arginine in place of glycine at position 130 results in local structural changes. The mutation does not affect the dimerization region, but does alter the packing of surface α-helix 2 comprised of residues 128-141.

Experimental Methods

Cloning and Site-directed Mutagenesis

The wildtype construct of residues 1-379 of AE1, designated pZZ3_WT, was readily available from previous work. The G130R mutation was introduced into this construct using a pair of primers:

Forward 5' GAC CTC CCT GGC TAG AGT GGC CAA CCA 3'

Reverse 5' TGG TTG GCC ACT CTA GCC AGG GAG GTC 3'

and designated as pZZ13_WT. The cysteineless mutants (pZZ3 and pZZ13) and single cysteine mutants were constructed by using the QuikChange Site-Directed Mutagenesis Kit (Stratagene, La Jolla, CA). The sequences of all mutants were checked by DNA sequencing.

Protein Preparation and On-Column Labeling

Plasmids were transformed into BL21 Gold (DE3) *E. coli* competent cells (Stratagene, La Jolla, CA). The auto-induction protocol developed by Dr. F. William Studier (Brookhaven National Laboratory) was used for the expression of cdb3 (Studier 2005). Overnight starter cultures were grown in PAG at 37°C and 200 μL of the starter cultures were used to inoculate 200 mL ZYP-5052 for overnight auto-induction (14 hours). Saturation (A_{600} = 4.8~7.0) was usually reached by 10 hours at 37°C. Additional incubation for 4 hours ensured maximum lactose auto-induction. His-tagged cdb3 purification was carried out using Ni-NTA resin as described by the manufacturer (Qiagen, Valencia, CA). Protein concentration was determined by UV absorption at 280 nm using an extinction coefficient of 33,000 $M^{-1}cm^{-1}$. Purity of the expressed proteins was checked by SDS-PAGE. Single cysteine mutants were spin-labeled with a 10-fold molar excess of 1-oxyl-2,2,5,5-tetramethyl-Δ3-pyrroline-3-methyl methanethiosulfonate spin label (MTSSL; Toronto Research Chemicals, North York, ON Canada) in the dark at room temperature for 2 hours and then overnight at 4°C in a buffer containing 50 mM NaH_2PO_4, 300 mM NaCl, and 200 mM imidazole, pH 8.0. Unbound label was removed from all samples by diluting and reconcentrating four times (~ 1:50 v/v) in an Amicon Ultra-4 Centrifugal Filter Device (30 kDa nominal molecular weight limit, Millipore, Bedford, MA) using a buffer containing 20 mM NaH_2PO_4, 100 mM NaCl, 1 mM EDTA, pH 6.8. All EPR measurements were collected with the spin-labeled samples in this buffer at pH 6.8. Spin-labeled protein concentrations were determined using double integration of CW-EPR measurements with a

1 mM 4-hydroxy-2,2,6,6-tetramethylpiperidine-N-oxyl (Tempol) standard. 3D structures were visualized using MacPyMOL (DeLano Scientific LLC, San Carlos, CA).

Experimental Results

G130R Mutant Dimer Remains Unperturbed

The crystal structure of cdb3 depicted a dimeric conformation at pH 4.8 (Zhang et al. 2000) that was confirmed by SDSL studies of the solution structure at neutral pH (Zhou et al. 2005). The dimerization arms span from residue 304 to 357 and consist of β-strand 11 situated between α-helixes 9 and 10. These elements interlock the two monomers through extensive backbone and side chain interactions (Zhang et al. 2000). To analyze the global structure and oligermerization of the G130R mutant, site directed spin labeling coupled with electron paramagnetic resonance (SDSL-EPR) was employed with and without the G130R mutation. Single cysteine mutants of residues both near the dimer interface and distributed around the peripheral globular domain were generated and spin labeled with MTSSL, designated as side chain R1 (Figure 12) (Berliner et al. 1982; Langen et al. 2000).

The spectra of most sites were showed little difference between the G130 and R130 backgrounds for all sites save two. The spectra of 105R1 showed only a small difference in lineshape while the fast motion of residue 277, found on the surface of the globular domain, is slightly dampened in the G130R mutant. Similar side chain mobility, lineshape components, and splitting was found for the remain-

ing sites studied- the highly mobile lineshape of 142R1, which is found at the start of the loop connecting helix 2 and helix 3; the immobilized lineshape of 290R1, which is situated on the interior surface of helix 7; the slightly mobile 312R1, which is located on the α-helix of the dimerization arm in the space between the two monomers; and the marked broadening and three-peak splitting of 108R1 due to dipolar coupling of the spin labels between the two monomers (Figure 12).

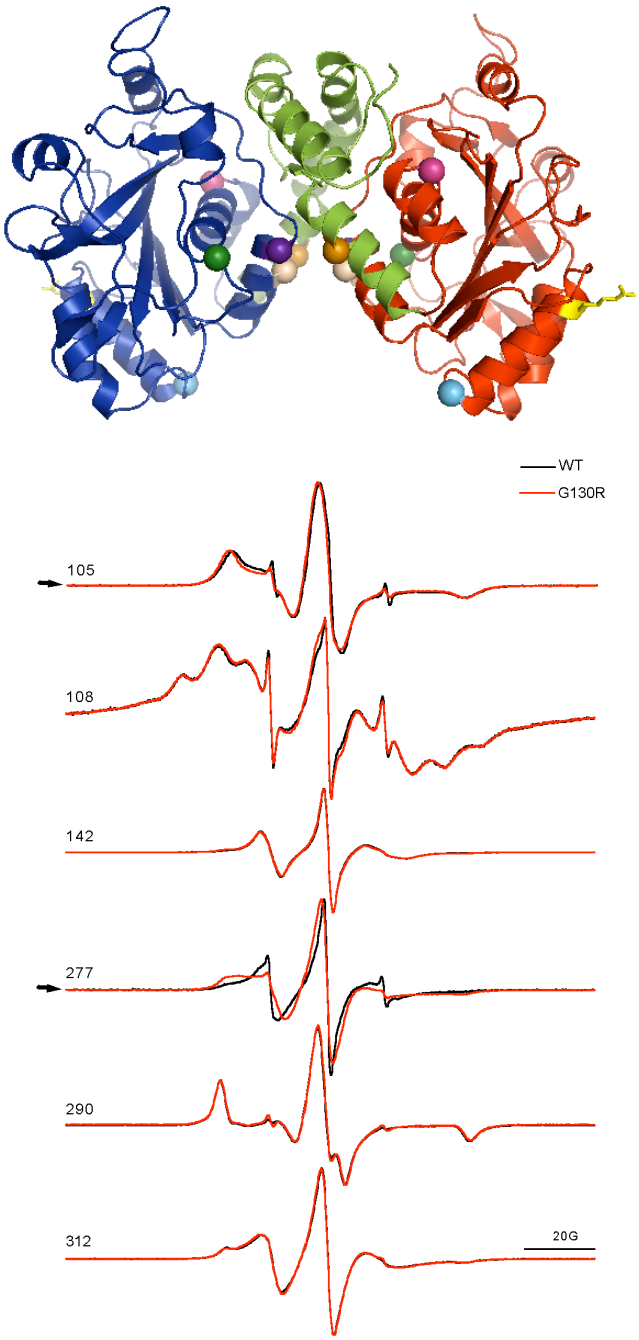

Figure 12. CW-EPR characterization of residues around the dimer interface

Top panel: Ribbon structure of cdb3 dimer with dimerization arms shown in light green and R130 in yellow stick. Cα atoms of spin-labeled residues are shown as spheres: 105 (dark purple), 108 (wheat), 142 (light blue), 277 (green), 290 (magenta), 312 (orange).

Bottom panel: EPR lineshapes of G130 cdb3 (black line) and R130 cdb3 (red line) with black arrows indicating spectra with observable differences. The 120 Gauss sweep spectra are normalized to the same amplitude for ease of comparison.

Further SDSL-EPR studies were performed on residues 339-345, found along the length of helix 10. These sites form part of the dimerization arm and follow an i to i + 3 pattern. Lineshapes are remarkably similar between the G130 and R130 backgrounds with each residue maintaining its original side chain mobility following the introduction of the G130R mutation (Figure 13). Two of these sites, 340R1 and 342R1 (Figure 14), were selected for double electron-electron resonance experiments, carried out by Dr. Eric Hustedt (Vanderbilt University, Nashville, TN). Results of these experiments showed no change in the intramolecular distances between either pair of residues (Figure 14). Together, these findings show the dimer interface remains unchanged in the G130R mutant.

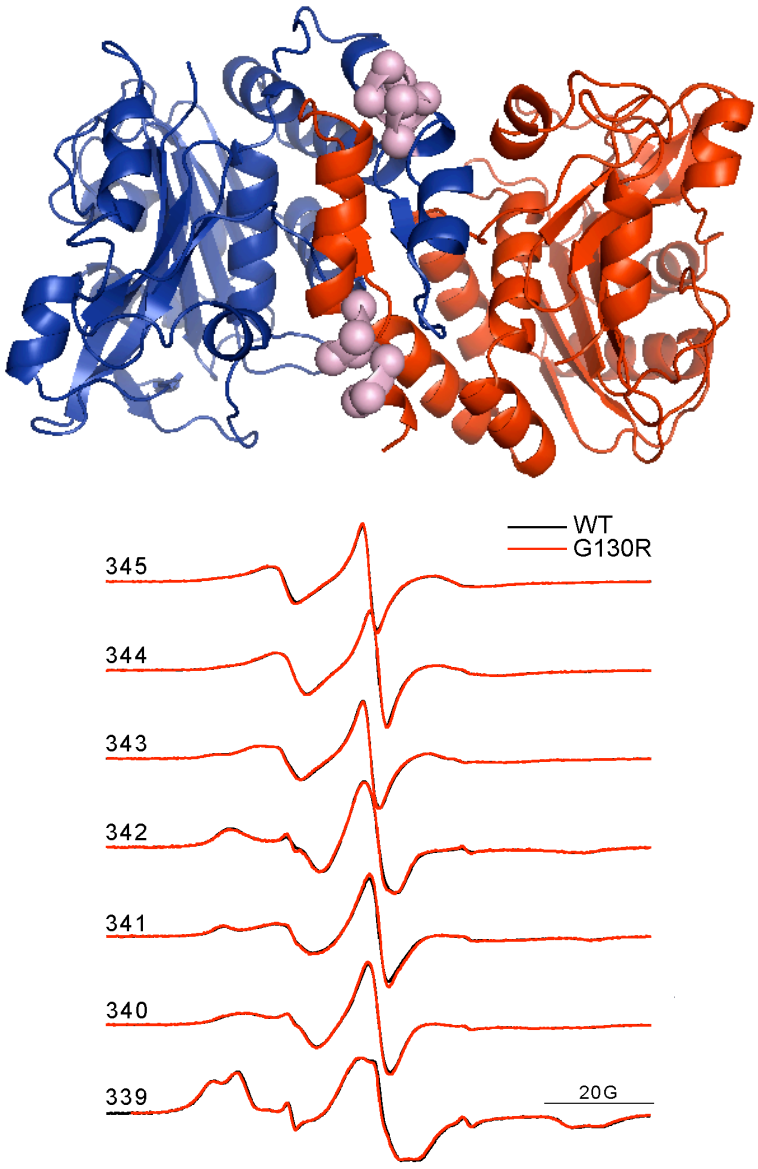

Figure 13. EPR characterization of residues 339-345 on the dimerization arms

Top panel: The structure and location of residues 339-345 (pink) on the ribbon diagram of the cdb3 dimer (blue and red).

Bottom panel: The CW-EPR spectrum at each position is normalized to the same amplitude and with a total scan width of 100 Gauss.

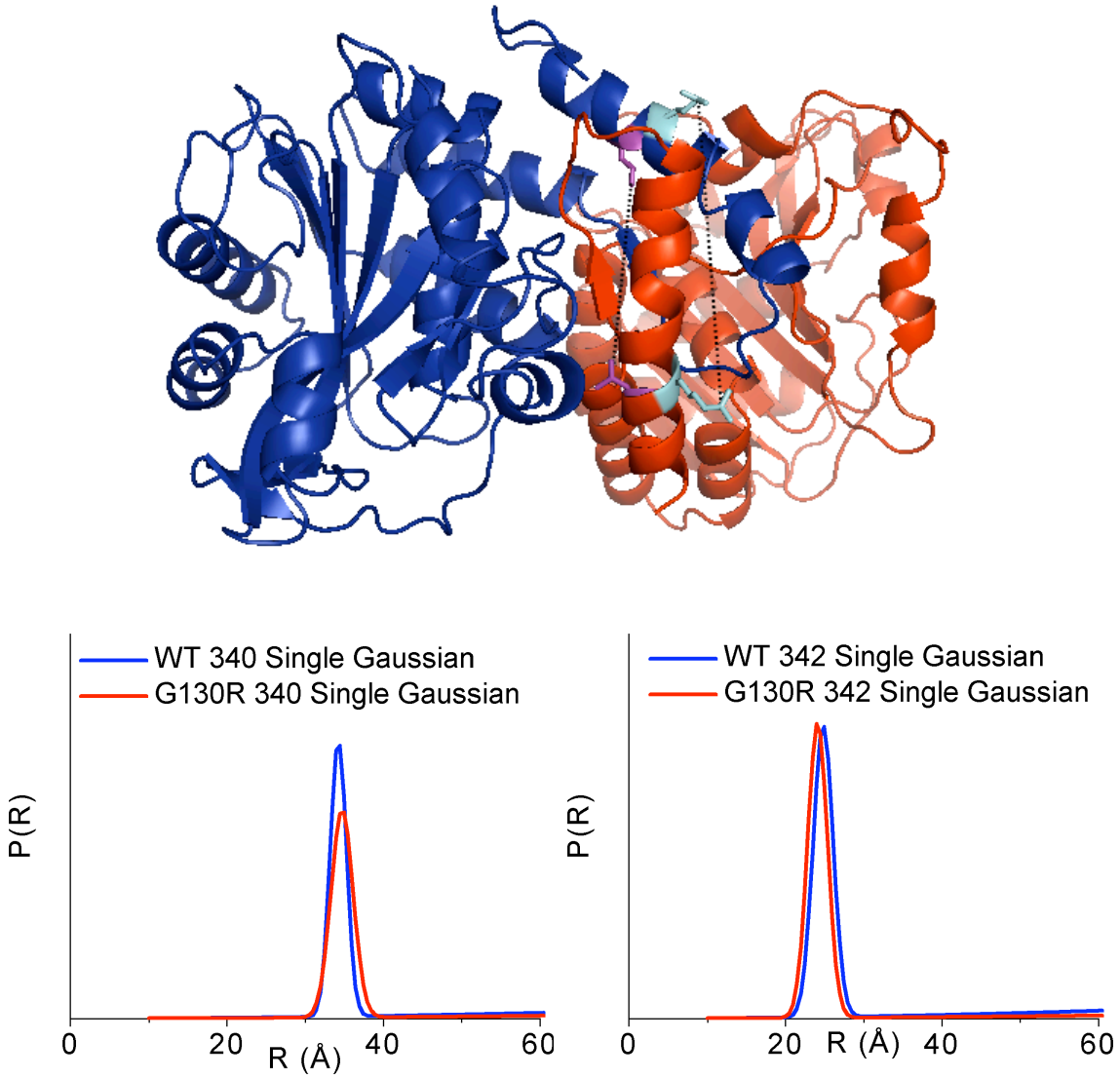

Figure 14. DEER characterization of residues 340 and 342 on the dimerization arms

Top panel: Set up for DEER experiments with residue 340 (cyan stick) and residue 342 (purple stick) spin labeled. Residue 340 is located on the surface while residue 342 is buried within the dimer interface. The dotted black line represents the intramolecular distances measured for each experiment.

Bottom panel: Analysis of DEER results for G130 cdb3 (blue) and R130 cdb3 (red) shows no significant change in either the magnitude or distribution of distances for site 340 (left) and 342 (right).

Structural Rearrangement in the α2 Surface Helix

While residue 130 faces out from the surface, making it less likely to be involved in the internal packing of the protein and the φ, ψ dihedral angles common to arginine are also agreeable to the helical secondary structure, the G130R mutation inserts a residue with very different steric and electrostatic properties. As such, the substituted arginine residue might disrupt or alter the normal folding of the surface helix. The local effects of the G130R mutation were studied by placing 10 R1 side chains along the N-terminal half of helix 2 (Figure 15). The purity of samples was checked with SDS-Page and concentrations determined by double integration of EPR signals.

Helix 2 of cdb3 is comprised of residues 128 to 141. CW-EPR spectra of single cysteine mutants from residue 127 to residue 137 showed differences in the lineshapes for residues 131-136 when comparing the normal cdb3 to the G130R mutant (Figure 15). The altered lineshapes indicate a change in the side chain mobilities of these residues for a portion of the G130R population. Residues 131, 132, 135, and 136 are found on the internal surface of helix 2 and residue 133 faces the solvent. Each of these residues show only slight changes in species populations with the G130R mutation, while residue 134 shows a more notable change. Following the introduction of the G130R mutation, a significant population of slower-moving species appears in addition to the typically fast-moving, solvent exposed species. Accessibility of residues 127 to 137 with the water soluble paramagnetic agent NiEDDA was measured using a dielectric resonator (Farahbakhsh et al. 1992; Hubbell et al. 1996). Solvent accessibility of the G130 and R130 backgrounds are plotted as a function of residue number (Figure 16). The accessibility

plot displays that the approximate periodicity of 4 characteristic of an a-helix is maintained in the G130R mutant. The frequency of collision between the spin label and paramagnetic agent is similar for these residues, suggesting that the overall tertiary environment of these residues remains the same with one side of the helix on the surface and the other facing the hydrophobic core. These results show that the backbone of helix 2 retains both its secondary structure and orientation.

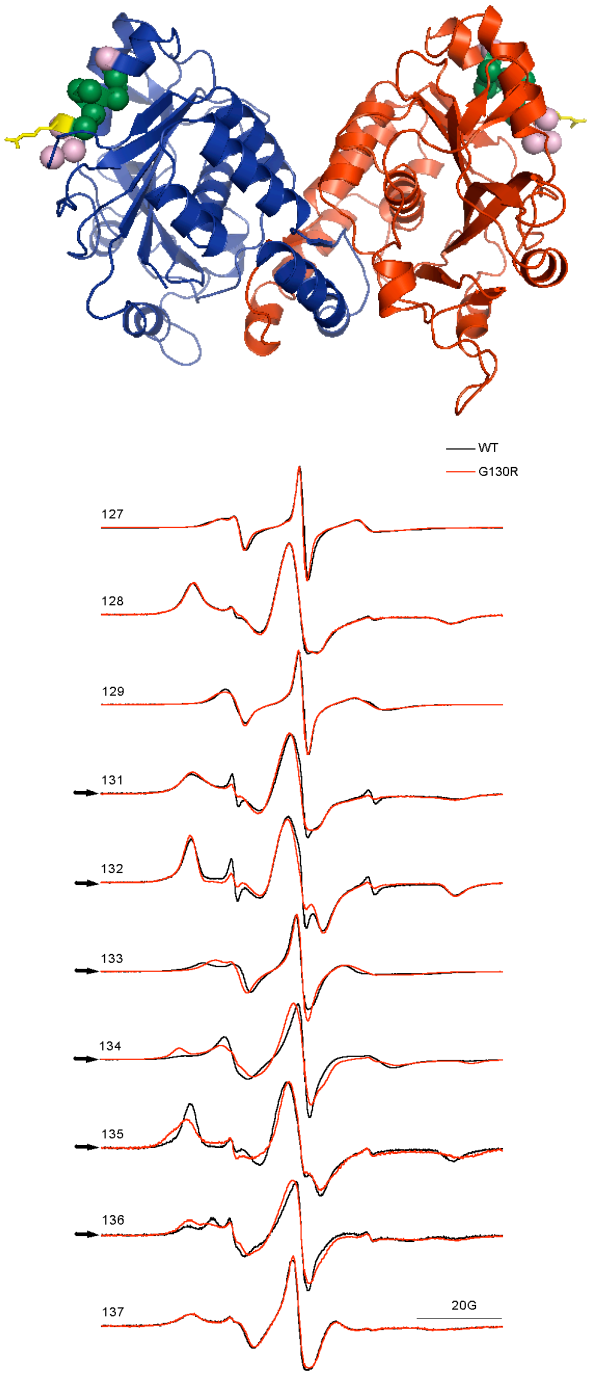

Figure 15. EPR characterization of residues 127-137 on helix 2

Top panel: Residues 127-129 and 137 (pink) and residues 131-136 (green) are displayed on a ribbon diagram of the cdb3 dimer. R130 is shown in yellow stick. The green spheres coincide with the residues that showed a shift in the EPR spectra from the wild type.

Bottom panel: 100 Gauss scans of residues 127-137 with normalized amplitudes. Arrows indicate spectrum that show changes between the G130 (black) and R130 (red) samples.

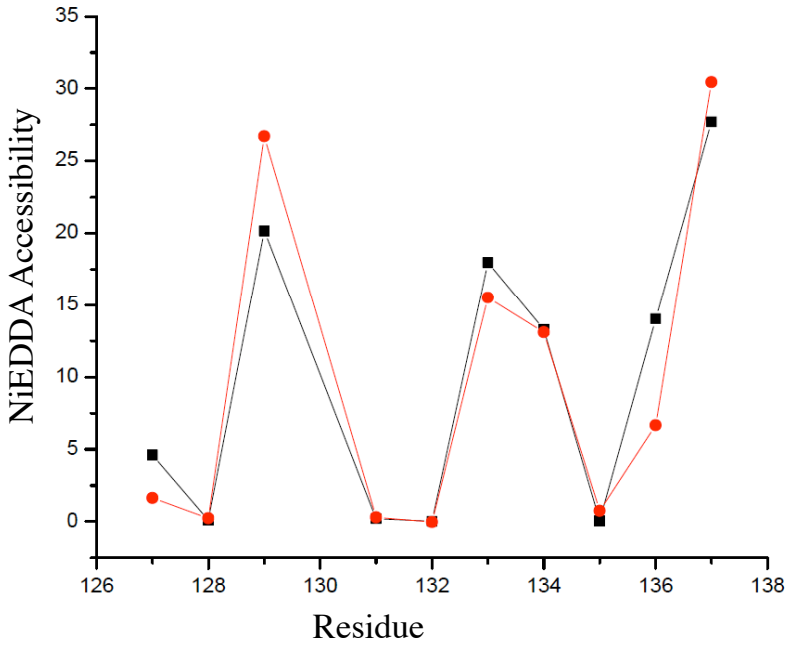

Figure 16. NiEDDA accessibility of the R1 side chain from residues 127-137

Black squares represent the NiEDDA accessibility of residues 127-137 of the wt-cdb3. Red circles represent the NiEDDA accessibility of residues 127-137 of the G130R mutant.

Discussion

As with many mutations linked to human disease, pathogenic mutations in AE1 can alter protein function in a number of different ways including abnormal biosynthesis levels, incorrect trafficking, misfolding, and functional defects. AE1 mutations are responsible for HS, SAO, and distal renal tubular acidosis (dRTA). The importance of cdb3's role as an organization center for various protein-protein interactions related to membrane stability and deformability is evidenced by the mutations in this domain that lead to diseases (HS, SAO) associated with membrane defects. The crystal structure of cdb3 (Zhang et al. 2000) and solution structure of cdb3 (Zhou et al. 2005) provide a means to deduce the structural significance of mutation sites that result in abnormal red blood cell shape but do not alter

band 3 expression. Substitution of the glycine at position 130 with arginine (designated as Band 3 Fukuoka) occurs at the solvent-exposed surface of helix 2, a part of the peripheral globular domain (Inoue et al. 1998). Sedimentation equilibrium, circular dichromism, and thermal denaturation experiments showed the G130R mutant maintained the same oligomerization state, secondary structure, and stability as the wild-type protein, indicating smaller scale structural changes (Bustos and Reithmeier 2006).

SDSL-EPR experiments, capable of analyzing of such changes to the environment and positioning of individual residues (Klug and Feix 2008), were utilized for the comparison of side chain mobility and solvent accessibility at various sites on both the wild type and G130R mutant. These locations were distributed through the globular domain, the dimer interface, or adjacent to the site of the mutation. The latter group of sites are immediately in the vicinity of the mutation site on helix 2.

As shown in the crystal structure, G130 is found on the solvent-accessible surface near the start of helix 2. Our data is in agreement with previous studies showing the global structure and dimer interface remain unchanged by the G130R mutation. With regards to the local backbone structure, arginine is unlikely to disrupt the structure of helix 2 by its substitution due to its ϕ, Ψ angles giving it a high propensity for involvement in right-handed helices. The electrostatic and steric qualities, on the other hand, are very different from glycine. Arginine is a long, flexible side chain with a positive charge, making it hydrophilic, whereas glycine is small and hydrophobic. As a solvent-exposed residue, such a substitution should not be unfavorable.

Replacing the glycine with an arginine would alter the local electrostatic field and that could cause the slight shift in the side chain interactions of nearby residues along helix 2. Simple inspection of the spectra reveals that while the spectral shape of both 131R1 and 132R1, the decrease in peak heights indicate slowed side chain motion. More notable are the changes in the spectra for 133R1 and 134R1. These two residues are both on the solvent-exposed side of the helix and the overall shape of their spectra reflect as such. The differences in the spectra, more specifically the appearance of a peak more representative of slow motion in the spectrum for 134R1 and an opposite shift in 133R1, are indicative of changes in the tertiary contacts for these residues. While the R1 side chain of 133 becomes more mobile, the R1 side chain for 134 increases the number of tertiary contacts. Residue 136 is buried on the hydrophobic side of the helix and its spectral appearance, while different between the wild type and mutant species, still approaches the rigid limit. 137R1 is the last side chain to exhibit a change in its spectrum, displaying an increased population with slower movement as well as a slight change in the central line. While the side chain mobility of these sites alters in some manner, the solvent accessibility does not. These data suggest that the helix does not undergo any manner of rotation though the side chain interactions change. This work highlights the use of SDSL-EPR in evaluating small structural changes and provides further information towards understanding the molecular pathophysiology of hereditary spherocytosis.

Further Work

Though these changes seen in the EPR data for the G130R mutation are subtle, the structural differences still result in altered protein-protein interactions, most notably is the loss of protein 4.2. Since protein 4.2 is believed to bind in the region of the dimerization arm, it is more likely that helix 2 influences the cdb3-ankyrin interaction, which stabilizes the binding of protein 4.2 with cdb3 (Rybicki et al. 1995). Ankyrin has been shown to interact with cdb3 on the surface opposite the dimer interface and modeling using the protein docking program 3D-Dock proposes the contact surface to include the α-helix 3, the loops connecting the first and second β-strands, the fifth β-strand and α-helix 2 that follows, along with β-strands six to ten and α-helix six (Figure 17) (Chang and Low 2003; Michaely et al. 2002). Further evidence for this surface as the ankyrin binding interface comes from site-directed fluorescence labeling (SDFL) that showed residues near helix 2 experienced a change in exposure upon binding of ankyrin to normal cdb3 (Figure 18 and Table 1) (Zhou thesis).

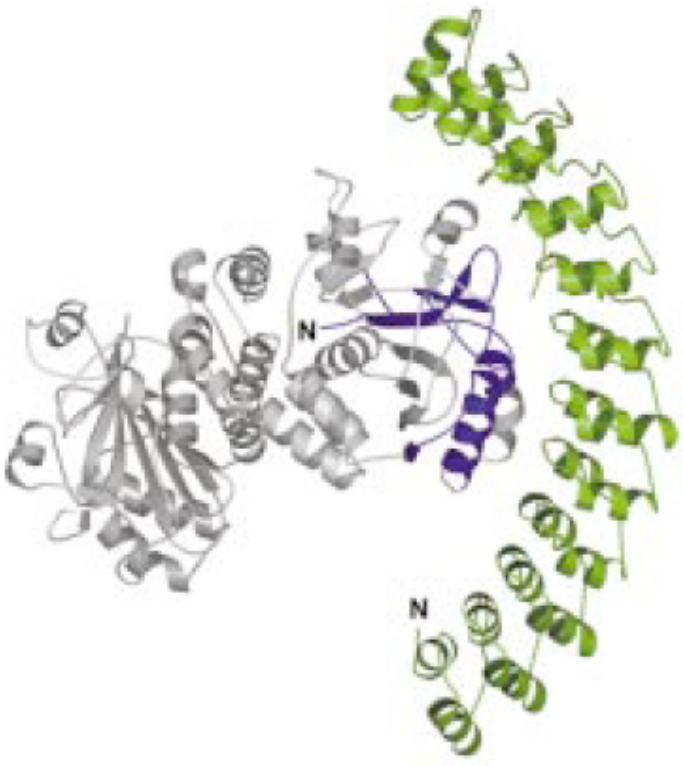

Figure 17. Model of the interaction between cdb3 and ankyrin

Ribbon diagram of the computer generated docking of ankyrin to cdb3. Ankyrin (green) interacts with the peripheral of cdb3's globular domain. The proposed binding site on cdb3 is displayed in dark purple while the rest of the dimer is displayed in gray. (Michaely et al. 2002)

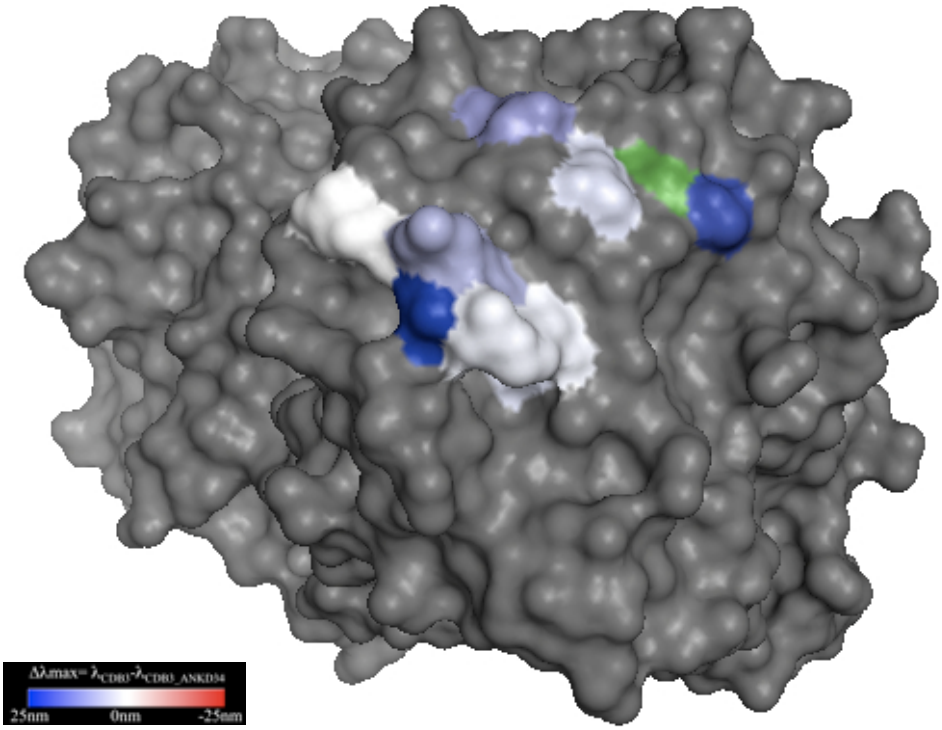

Figure 18. Ankyrin-binding interface mapped on the cdb3 dimer

Surface rendering of the cdb3 dimer structured. The colored legend bar displays the linear-gradient scale of blue or red shift of the maximum emission wavelength (λmax) upon ankyrin binding. Residue 130 is displayed in green. Residues tested on the same face of the globular domain are colored according to the values of Δλmax (Table 1).

Table 1. λmax shift upon ANK_D34 of cdb3

Residue #	127	133	137	148	151	152	155	156
λ_{cdb3} (nm)	536	531	526	531	521	524	527	503
$\lambda_{cdb3+ANK\_D34}$ (nm)	516	527	514	531	512	499	525	499
$\Delta\lambda_{max} = \lambda_{cdb3} - \lambda_{cdb3+ANK\_D34}$ (nm)	20	4	12	0	9	25	2	4

Since the G130R mutation is located on the surface-exposed side of helix 2, it provides an opportunity to better understand the interaction between cdb3 and ankyrin. For this purpose, we plan to use SDSL-EPR experiments in order to study the role of helix 2 in the binding of ankyrin. CW-EPR experiments with cdb3 in the presence of ankyrin can provide a glimpse at the tertiary contacts to residues along helix 2 and how these contacts may change in the G130R mutant. Quantitative analysis of spin label mobility could also be useful in gauging the interaction between specific residue side chains on cdb3 with ankyrin. Perhaps more informative, however, would be the use of NiEDDA accessibility studies to examine the solvent exposure of cdb3 upon binding ankyrin. For wild type cdb3, one would expect that the surface residues of helix 2 would become less exposed if they are involved in the interface with ankyrin. Structural rearrangements upon binding, for example if the helix rotates, can also be observed based on the pattern of solvent accessibility. Comparing the changes with the wild type cdb3 and the G130R mutant in both the presence of ankyrin can provide information on how the small structural changes seen in this work affect helix 2 as part of the binding surface.

REFERENCES

Agre, P., Orringer, E.P., and Bennett, V. (1982) Deficient red-cell spectrin in severe, recessively inherited spherocytosis. *N Engl J Med*, **306**(19):1155-61.

Altenbach, C., Froncisz, W., Hyde, J.S., and Hubbell, W.L. (1989) Conformation of spin-labeled melittin at membrane surfaces investigated by pulse saturation recovery and continuous wave power saturation electron paramagnetic resonance. *Biophys J*, **56**(6):1183-91.

Altenbach, C., Oh, K.J., Trabanino, R.J., Hideg, K., and Hubbell, W.L. (2001) Estimation of inter-residue distances in spin labeled proteins at physiological temperatures; experimental strategies and practical limitations. *Biochemistry*, **40**(51):15483-92.

Anong, W.A., Weis, T.L., and Low, P.S. (2006) Rate of rupture and reattachment of the band 3-ankyrin bridge on the human erythrocyte membrane. *J Biol Chem*, **281**(31):22360-6.

Bennett, V. (1989) The spectrin-actin junction of erythrocyte membrane skeletons. *Biochim Biophys Acta*, **988**(1):107-21.

Bennett, V. and Stenbuck, P.J. (1979) The membrane attachment protein for spectrin is associated with band 3 in human erythrocyte membranes. *Nature*, **280**(5722):468-73.

Bennett, V. and Stenbuck, P.J. (1980) Association between ankyrin and the cytoplasmic domain of band 3 isolated from the human erythrocyte membrane. *J Biol Chem*, **255**(13)6424-32.

Berlinger, L.J., Grunwald, J., Hankovsky, H.O., and Hideg, K. (1982) A novel reversible thiol-specific spin label: papain active site labeling and inhibition. *Anal Biochem*, **119**(2):450-5.

Beth, A.H., Balasubramanian, K., Wilder, R.T., Venkataramu, S.D., Robinson, B.H., Dalton, L.R., Pearson, D.E., and Park, J.H. (1981) Structural and motional changes in glyceraldehyde-3-phosphate dehydrogenase upon binding to the band 3 protein of the erythrocyte membrane examined with [15N,2H]maleimide spin label and electron paramagnetic resonance. *Proc Natl Acad Sci U S A*, **78**(8):4955-9.

Blackman, S.M., Hustedt, E.J., Cobb, C.E., and Beth, A.H. (2001) Flexibility of the cytoplasmic domain of the anion exchange protein, band 3, in human erythrocytes. *Biophys J*, **81**(6):3363-76.

Brody, J.P., Han, Y., Austin, R.H., and Bitensky, M. (1995) Deformation and flow of red blood cells in a synthetic lattice: evidence for an active cytoskeleton. *Biophys J*, **68**(6):2224-32.

Bustos, S.P. and Reithmeier, R.A. (2006) Structure and stability of hereditary spherocytosis mutants of the cystolic domain of the erythrocyte anion exchanger 1 protein. *Biochemistry*, **45**(3):1026-34.

Cabantchik, Z.I. and Rothstein, A. (1974) Membrane proteins related to anion permeability of human red blood cells. I. Localization of disulfonic stilbene binding sites in proteins involved in permeation. *J Membr Biol*, **15**(3):207-26.

Campanella, M.E., Chu, H., and Low, P.S. (2005) Assembly and regulation of a glycolytic enzyme complex on the human erythrocyte membrane. *Proc Natl Acad Sci U S A*, **102**(7):2402-7.

Chang, S.H. and Low, P.S. (2003) Identification of a critical ankyrin-binding loop on the cytoplasmic domain of erythrocyte membrane band 3 by crystal structure analysis and site-directed mutagenesis. *J Biol Chem*, **278**(9):6879-84.

Chasis, J.A. and Mohandas, N. (1986) Erythrocyte membrane deformability and stability: two distinct membrane properties that are independently regulated by skeletal protein associations. *J Cell Biol*, **103**(2):343-50.

Columbus, L. and Hubbell, W.L. (2002) A new spin on protein dynamics. *Trends Biochem Sci*, **27**(6):288-95.

Columbus, L., Kálai, T., Jekö, J., Hideg, K., and Hubbell, W.L. (2001) Molecular motion of spin labeled side chains in alpha-helices: analysis by variation of side chain structure. *Biochemistry*, **40**(13):3828-46.

Crandall, E.D., Mathew, S.J., Fleischer, R.S., Winter, H.I., and Bidani, A. (1981) Effects of inhibition of RBC HCO_3^-/Cl^- exchange on CO_2 excretion and downstream pH disequilibrium in isolated rat lungs. *J Clin Invest*, **68**(4):853-62.

Davis, L., Lux, S.E., and Bennett, V. (1989) Mapping the ankyrin-binding site of the human erythrocyte anion exchanger. *J Biol Chem*, **264**(16):9665-72.

Dacie, J.V. and White, J.C. (1949) Erythropoiesis with particular reference to its study by biopsy of human bone marrow: a review. *J Clin Pathol*, **2**(1):1-32.

Delaunay, J. (2002) Molecular basis of red cell membrane disorders. *Acta Haematol*, **108**(4):210-8.

Dhermy, D., Burnier, O., Bourgeois, M., and Grandchamp, B. (1999) The red blood cell band 3 variant (band 3 Biceêtrel:R490C) associated with dominant hereditary spherocytosis causes defective membrane targeting of the molecule and a dominant negative effect. *Mol Membr Biol*, **16**(4):305-12.

Fairbanks, G., Steck, T.L., and Wallach, D.F. (1971) Electrophoretic analysis of the major polypeptides of the human erythrocyte membrane. *Biochemistry*, **10**(13):2606-17.

Farahbakhsh, Z.T., Altenbach, C., and Hubbell, W.L. (1992) Spin labeled cysteines as sensors for protein-lipid interaction and conformation in rhodopsin. *Photochem Photobiol*, **56**(6):1019-33.

Farrens, D.L., Altenbach, C., Yang, K., Hubbell, W.L., and Khorana, H.G. (1996) Requirement of rigid-body motion of transmembrane helices for light activation of rhodopsin. *Science*, **274**(5288):768-70.

Furuya, W., Tarshis, T., Law, F.Y., and Knauf, P.A. (1984) Transmembrane effects of intracellular chloride on the inhibitory potency of extracellular H_2DIDS. Evidence for two conformations of the transport site of the human erythrocyte anion exchanger protein. *J Gen Physiol*, **83**(5):657-81.

Galtieri, A., Tellone, E., Romano, L., Misiti, F., Bellocco, E., Ficarra, S., Russo, A., Di Rosa, D., Castagnola, M., Giardina, B., and Messana, I. (2002) Band-3 protein function in human erythrocytes: effect of oxygenation-deoxygenation. *Biochim Biophys Acta*, **1564**(1):214-8.

Groves, J.D. and Tanner, M.J. (1999) Structural model for the organization of the transmembrane spans of the human red-cell anion exchanger (band 3;AE1). *Biochem J*, **344** Pt 3:699-711.

Harrison, M.L., Isaacson, C.C., Burg, D.L., Geahlen, R.L., and Low, P.S. (1994) Phosphorylation of human erythrocyte band 3 by endogenous p72syk. *J Biol Chem*, **269**(2):955-9.

Hubbell, W.L., Mchaourab, H.S., Altenbach, C., and Lietzow, M.A. (1996) Watching proteins move using site-directed spin labeling. *Structure*, **4**(7):779-83.

Hustedt, E.J., Smirnov, A.I., Laub, C.F., Cobb, C.E., and Beth, A.H. (1997) Molecular distances from dipolar coupled spin-labels: the global analysis of multi-frequency continuous wave electron paramagnetic resonance data. *Biophys J*, **72**(4):1861-77.

Hustedt, E.J. and Beth, A.H. (1999) Nitroxide spin-spin interactions: application to protein structure and dynamics. *Annu Rev Biophys Biomol Struct*, **28**:129-53.

Inoue, T., Kanzaki, A., Kaku, M., Yawata, A., Takezono, M., Okamoto, N., Wada, H., Sugihara, T., Yamada, O., Katayama, Y., Nagata, N., and Yawata, Y. (1998) Homozygous missense mutation (band 3 Fukuoka: G130R): a mild form of hereditary spherocytosis with near-normal band 3 content and minimal changes of membrane ultrastructure despite moderate protein 4.2 deficiency. *Br J Haematol*, **102**(4):932-9.

Jarolim, P., Palenk, J., Amato, D., Hassan, K., Sapak, P., Nurse, G.T., Rubin, H.L., Zhai, S., Sahr, K.E., and Liu, S.C. (1991) Deletion in erythrocyte band 3 gene in malaria-resistant Southeast Asian ovalocytosis. *Proc Natl Acad Sci U S A*, **88**(24):11022-6.

Jarolim, P., Palek, J., Rubin, H.L., Prchal, J.T., Korsgren, C., and Cohen, C.M. (1992) Band 3 Tuscaloosa: Pro327----Arg327 substitution in the cytoplasmic domain of erythrocyte band 3 protein associated with spherocytic hemolytic anemia and partial deficiency of protein 4.2. *Blood*, **80**(2):523-9.

Jarolim, P., Murray, J.L., Rubin, H.L., Taylor, W.M., Prchal, J.T., Ballas, S.K., Snyder, L.M., Chrobak, L., Melrose, W.D., Brabec, V., and Palek, J. (1996) Characterization of 13 novel band 3 gene defects in hereditary spherocytosis with band 3 deficiency. *Blood*, **88**(11):4366-74.

Jenkins, J.D, Kezdy, F.J., and Steck, T.L. (1985) Mode of interaction of phosphofructokinase with the erythrocyte membrane. *J Biol Chem*, **260**(19):20426-33.

Kimura, F., Ito, H., Shimizu, H., Togawa, A., Otsuka, M., Yoshidome, H., Shimamura, F., Kato, A., Nukui, Y., Ambiru, S., and Miyazaki, M. (2003) Partial splenic embolization for the treatment of hereditary spherocytosis. *AJR Am J Roentgenol*, **181**(4):1021-4.

Klug, C.S. and Feix, J.B. (2008) Methods and applications of site-directed spin labeling EPR spectroscopy. *Methods Cell Biol*, **84**:617-58.

Korsgren, C. and Cohen, C.M. (1988) Associations of human erythrocyte band 4.2. Binding to ankyrin and to the cytoplasmic domain of band 3. *J Biol Chem*, **263**(21):10212-8.

Kumar, V., Abbas, A., and Fausto, N. *Robbins and Cotran Pathological Basis of Disease, 8th Ed.* Saunders: 2009.

Langen, R., Oh, K.J., Cascio, D., and Hubbell, W.L. (2000) Crystal structures of spin labeled T4 lysozyme mutants: implications for the interpretation of EPR spectra in terms of structure. *Biochemistry*, **39**(29):8396-405.

Law, R., Carl, P., Harper, S., Dalhaimer, P., Speicher, D.W., and Discher, D.E. (2003) Cooperativity in forced unfolding of tandem spectrin repeats. *Biophys J*, **84**(1):533-44.

Liu, S.C., Derick, L.H., and Palek, J. (1987) Visualization of the hexagonal lattice in the erythrocyte membrane skeleton. *J Cell Biol*, **104**(3):527-36.

Liu, F., Mizukami, H., Sarnaik, S., and Ostafin, A. (2005) Calcium-dependent human erythrocyte cytoskeleton stability analysis through atomic force microscopy. *J Struct Biol*, **150**(2):200-10.

Low, P.S. (1986) Structure and function of the cytoplasmic domain of band 3: center of erythrocyte membrane-peripheral protein interactions. *Biochim Biophys Acta*, **864**(2):145-67.

Low, P.S., Willardson, B.M., Mohandas, N., Rossi, M., and Shohet, S. (1991) Contribution of the band 3-ankyrin interaction to erythrocyte membrane mechanical stability. *Blood*, **77**(7):1581-6.

Low, P.S., Rathinavelu, P., and Harrison, M.L. (1993) Regulation of glycolysis via reversible enzyme binding to the membrane protein, band 3. *J Biol Chem*, **268**(20):14627-31.

Lux, S.E., John, K.M., Kopito, R.R, and Lodish, H.F. (1989) Cloning and characterization of band 3, the human erythrocyte anion-exchanger protein (AE1). *Proc Natl Acad Sci U S A*. **86**(23):9089-93.

Mchaourab, H.S., Leitzow, M.A., Hideg, K., and Hubbell, W.L. (1996) Motion of spin-labeled side chains in T4 lysozyme. Correlation with protein structure and dynamics. *Biochemistry*, **35**(24):7692-704.

MacDonald, R.I. and Cummings, J.A. (2004) Stabilities of folding clustered, two-repeat fragments of spectrin reveal a potential hinge in the human erythroid spectrin tetramer. *Proc Natl Acad Sci U S A*, **101**(6):1502-7.

Maillet, P., Alliosio, N., Morlé, L., and Delaunay, J. (1996) Spectrin mutations in hereditary elliptocytosis and hereditary spherocytosis. *Hum Mutat*, **8**(2):97-107.

Michaely, P., Tomchick, D.R., Machius, M., and Anderson, R.G. (2002) Crystal structure of a 12 ANK repeat stack from human ankyrinR. *EMBO J*, **21**(23):6387-96.

Mohandas, N., Winardi, R., Knowles, D., Leung, A., Parra, M., George, E., Conboy, J., and Chasis, J. (1992) Molecular basis for membrane rigidity of hereditary ovalocytosis. A novel mechanism involving the cytoplasmic domain of band 3. *J Clin Invest*, **89**(2):686-92.

Morinis, J., Dutta, S., Blanchette, V., Butchart, S., and Langer, J.C. (2008) Laparoscopic partial vs total splenectomy in children with hereditary spherocytosis. *J Pediatr Surg*, **43**(9):1649-52.

Morrow, J.S. and Marchesi, V.T. (1981) Self-assembly of spectrin oligomers in vitro: a basis for a dynamic cytoskeleton. *J Cell Biol*, **88**(2):463-8.

Murthy, S.N., Liu, T., Kaul, R.K., Köhler, H., and Steck, T.L. (1981) The aldolase-binding site of the human erythrocyte membrane is at the NH_2 terminus of band 3. *J Biol Chem*, **256**(21):11203-8.

Pasternack, G.R., Anderson, R.A., Leto, T.L., and Marchesi, V.T. (1985) Interactions between protein 4.1 and band 3. An alternative binding site for an element of the membrane skeleton. *J Biol Chem*, **260**(6):3676-83.

Perrotta, S., Gallagher, P.G., and Mohandas, N. (2008) Hereditary spherocytosis. *Lancet*, **372**(9647):1411-26.

Perozo, E., Cortes, D.M., Sompornpisut, P., Kloda, A., and Martinac, B. (2002) Open channel structure of MscL and the gating mechanism of mechanosensitive channels. *Nature*, **418**(6901):942-8.

Peters, L.L., Shivdasani, R.A., Liu, S.C., Hanspal, M., John, K.M., Gonzalez, J.M., Brugnara, C., Gwynn, B., Mohandas, N., Alper, S.L., Orkin, S.H., and Lux, S.E. (1996) Anion exchanger 1 (band 3) is required to prevent erythrocyte membrane surface loss but not to for the membrane skeleton. *Cell*, **86**(6):917-27.

Quilty, J.A. and Reithmeier, R.A. (2000) Trafficking and folding defects in hereditary spherocytosis mutants of the human red cell anion exchanger. *Traffic*, **1**(12):987-98.

Rief, M., Pascual, J., Saraste, M., and Gaub, H.E. (1999) Single molecule force spectroscopy of spectrin repeats: low unfolding forces in helix bundles. *J Mol Biol*, **286**(2):553-61.

Rogalski, A.A., Steck, T.L., and Waseem, A. (1989) Association of glyceraldehyde-3-phosphate dehydrogenase with the plasma membrane of the intact human red blood cell. *J Biol Chem*, **264**(11):6438-46.

Rybicki, A.C., Heath, R., Wolf, J.L., Lubin, B., and Schwartz, R.S. (1988) Deficiency of protein 4.2 in erythrocytes from a patient with Combs negative hemolytic anemia. Evidence for a role of protein 4.2 in stablizing ankyrin on the membrane. J Clin Invest, 81(3):893-901.

Rybicki, A.C., Musto, S., and Schwartz, R.S. (1995) Decreased content of protein 4.2 in ankyrin-deficient normoblasts (nb/nb) mouse red blood cells: evidence for ankyrin enhancement of protein 4.2 membrane binding. Blood, 86(9):3583-9.

Salomao, M., Zhang, X., Yang, Y., Lee, S., Hartwig, J.H., Chasis, J.A., Mohandas, N., and An, X. (2008) Protein 4.1R-dependent multiprotein complex: new insights into the structural organization of the red blood cell membrane. *Proc Natl Acad Sci U S A*, **105**(23):8026-31.

Silbernagl, S. and Despopoulos, A. *Color Atlas of Physiology, 6th Ed.* Thieme: 2009.

Skalak, R. and Branemark, P.I. (1969) Deformation of red blood cells in capillaries. *Science*, **164**(880):717-9.

Speicher, D.W. and Marchesi, V.T (1984) Erythrocyte spectrin is compromised of many homologous triple helical segments. *Nature*, **311**(5982):177-80.

Steck, T.L., Ramos, B., and Strapazon, E. (1976) Proteolytic dissection of band 3, the predominant transmembrane polypeptide of the human erythrocyte membrane. *Biochemistry*, **15**(5):1153-61.

Steinhoff, H.J., Radzwill, N., Thevis, W., Lenz, V., Brandenburg, D., Antson, A., Dodson, G., and Wollmer, A. (1997) Determination of interspin distances between spin labels attached to insulin: comparison of electron paramagnetic resonance data with the X-ray structure. *Biophys J*, **73**(6):3287-98.

Stoehr, G.A., Stauffer, U.G., and Eber, S.W. (2005) Near-total splenectomy: a new technique for the management of hereditary spherocytosis. *Ann Surg*, **241**(1):40-7.

Studier, F.W. (2005) Protein production by auto-induction in high density shaking cultures. *Protein Expr Purif*, **41**(1):207-34.

Su, Y., Ding, Y., Jiang, M., Jiang, W., Hu, X., and Zhang, Z. (2006) Associations of protein 4.2 with band 3 and ankyrin. *Mol Cell Biochem*, **289**(1-2):159-66.

Subczynski, W.K. and Hyde, J.S. (1981) The diffusion-concentration product of oxygen in lipid bilayers using the spin-label T1 method. *Biochim Biophys Acta*, **643**(2):283-91.

Takakuwa, Y. and Mohandas, N. (1988) Modulation of erythrocyte membrane material properties by Ca^{2+} and calmodulin. Implication for their role in the regulation of skeletal protein interactions. *J Clin Invest*, **82**(2):394-400.

Teti, D., Venza, I., Crupi, M., Busà, M., Loddo, S., and Romano, L. (2002) Anion transport in normal erythrocytes, sickle red cells, and ghosts in relation to hemoglobins and magnesium. *Arch Biochem Biophys*, **403**(2):149-54.

Toye, A.M., Williamson, R.C., Khanfar, M., Bader-Meunier, B., Cynober, T., Thibault, M., Tchernia, G., Déchaux, M., Delaunay, J., and Bruce, L.J. (2008) Band 3 Courcouronnes (Ser667Phe): a trafficking mutant differentially rescued by wild-type band 3 and glycophorin A. *Blood*, **111**(11):5380-9.

Uyesaka, N., Hasegawa, S., Ishioka, N., Ishioka, R., Shio, H., and Schechter, A.N. (1992) Effects of superoxide anions on red cell deformability and membrane proteins. *Biorheology*, **29**(2-3):217-29.

Walder, J.A., Chatterjee, R., Steck, T.L., Low, P.S., Musso, G.F., Kaiser, E.T., Rogers, P.H., and Arnone, A. (1984) The interaction of hemoglobin with the cytoplasmic domain of band 3 of the human erythrocyte membrane. *J Biol Chem*, **259**(16):10238-46.

Waugh, R.E. (1987) Effects of inherited membrane abnormalities on the viscoelastic properties of erythrocyte membrane. *Biophys J*, **51**(3):363-9.

Waugh, S.M. and Low, P.S. (1985) Hemichrome binding to band 3: nucleation of Heinz bodies on the erythrocyte membrane. *Biochemistry*, **24**(1):34-9.

Weber, R.E., Voelter, W., Fago, A., Echner, H., Campanella, E., and Low, P.S. (2004) Modulation of red cell glycolysis: interactions between vertebrate hemoglobins and cytoplasmic domains of band 3 red cell membrane proteins. *Am J Physiol Regul Integr Comp Physiol*, **287**(2):R454-64.

Zhang, D., Kiyatkin, A., Bolin, J.T, and Low, P.S. (2000) Crystallographic structure and functional interpretation of the cytoplasmic domain of erythrocyte membrane band 3. *Blood*, **96**(9):2925-33.

Zhou, Z., DeSensi, S.C., Stein, R.A., Brandon, S., Dixit, M., McArdle, E.J., Warren, E.M., Kroh, H.K., Song, L., Cobb, C.E., Hustedt, E.J., and Beth, A.H. (2005) Solution structure of the cytoplasmic domain of erythrocyte membrane band 3 determined by site-directed spin labeling. *Biochemistry*, **44**(46):15115-28.

Zhou, Z., DeSensi, S.C., Stein, R.A., Brandon, S., Song, L., Cobb, C.E., Hustedt, E.J., and Beth, A.H. (2007) Structure of the cytoplasmic domain of erythrocyte band 3 hereditary spherocytosis variant P327R: band 3 Tuscaloosa. *Biochemistry*, **46**(36):10248-57.

Zhu, Q., Lee, D.W., and Casey, J.R. (2003) Novel topology in C-terminal region of human plasma membrane protein, AE1. *J Biol Chem*, **278**(5):3112-20.